Curtailing the dark side in non-standard neutrino interactions

Coloma, Pilar; Denton, Peter B.; Gonzalez-Garcia, M. C.; Maltoni, Michele; Schwetz, Thomas

Published in:
Journal of High Energy Physics

DOI:
10.1007/JHEP04(2017)116

Publication date:
2017

Document version
Publisher's PDF, also known as Version of record

JHEP

Published for SISSA by Springer

Received: February 3, 2017
Revised: March 14, 2017
Accepted: April 13, 2017
Published: April 20, 2017

Curtailing the dark side in non-standard neutrino interactions

Pilar Coloma,[a] **Peter B. Denton,**[a,b,1] **M.C. Gonzalez-Garcia,**[c,d,e] **Michele Maltoni**[f] **and Thomas Schwetz**[g]

[a] *Theoretical Physics Department, Fermi National Accelerator Laboratory, P.O. Box 500, Batavia, IL 60510, U.S.A.*

[b] *Niels Bohr International Academy, University of Copenhagen, The Niels Bohr Institute, Blegdamsvej 17, DK-2100, Copenhagen, Denmark*

[c] *Departament de Fisíca Quàntica i Astrofísica and Institut de Ciencies del Cosmos, Universitat de Barcelona, Diagonal 647, E-08028 Barcelona, Spain*

[d] *Institució Catalana de Recerca i Estudis Avançats (ICREA), Pg. Lluis Companys 23, 08010 Barcelona, Spain*

[e] *C.N. Yang Institute for Theoretical Physics, Stony Brook University, Stony Brook, NY 11794-3840, U.S.A.*

[f] *Instituto de Física Teórica UAM/CSIC, Universidad Autónoma de Madrid, Calle de Nicolás Cabrera 13–15, Cantoblanco, E-28049 Madrid, Spain*

[g] *Institut für Kernphysik, Karlsruher Institut für Technologie (KIT), D-76021 Karlsruhe, Germany*

E-mail: pcoloma@fnal.gov, peterbd1@gmail.com, maria.gonzalez-garcia@stonybrook.edu, michele.maltoni@csic.es, schwetz@kit.edu

Abstract: In presence of non-standard neutrino interactions the neutrino flavor evolution equation is affected by a degeneracy which leads to the so-called LMA-Dark solution. It requires a solar mixing angle in the second octant and implies an ambiguity in the neutrino mass ordering. Non-oscillation experiments are required to break this degeneracy. We perform a combined analysis of data from oscillation experiments with the neutrino scattering experiments CHARM and NuTeV. We find that the degeneracy can be lifted if the non-standard neutrino interactions take place with down quarks, but it remains for up quarks. However, CHARM and NuTeV constraints apply only if the new interactions take place through mediators not much lighter than the electroweak scale. For light mediators we consider the possibility to resolve the degeneracy by using data from future coherent neutrino-nucleus scattering experiments. We find that, for an experiment using a stopped-pion neutrino source, the LMA-Dark degeneracy will either be resolved, or the presence of new interactions in the neutrino sector will be established with high significance.

Keywords: Neutrino Physics, Beyond Standard Model

ArXiv ePrint: 1701.04828

[1] ORCID: 0000-0002-5209-872X.

doi:10.1007/JHEP04(2017)116

Contents

JHEP04(2017)116

1 Introduction

Experiments measuring the flavor composition of solar and atmospheric neutrinos, as well as neutrinos produced in nuclear reactors and in accelerators, have established that lepton flavor is not conserved in neutrino propagation. Instead, it oscillates with a wavelength which depends on distance and energy, because neutrinos are massive and the mass states are admixtures of the flavor states [1–3]. At present all confirmed oscillation signatures can be well described with the three flavor neutrinos (ν_e, ν_μ, ν_τ) being quantum superpositions — all three with no-vanishing projections — of three massive states ν_i ($i = 1, 2, 3$) with masses m_i leading to two distinctive splittings (see ref. [4] for the latest determination of the neutrino masses and mixings).

Under the assumption that the Standard Model (SM) is the low energy effective model of a complete high energy theory, neutrino masses emerge naturally as the first observable consequence from higher dimensional operators. It is particularly remarkable that the only dimension five ($d = 5$) operator that can be built within the SM particle content is indeed the Weinberg operator [5], which after electroweak symmetry breaking leads to a suppression of neutrino masses with the scale of new physics Λ, as $m_\nu \sim \mathcal{O}(v^2/\Lambda) \ll v$,

where v is the Higgs vacuum expectation value. In this framework higher dimensional operators may also lead to observable consequences at low energies in the neutrino sector. At $d = 6$ these include four-fermion interactions involving neutrinos:

$$(\bar{\nu}_\alpha \gamma_\mu P_L \nu_\beta)(\bar{f}\gamma^\mu P f)\,, \tag{1.1}$$

or

$$(\bar{\nu}_\alpha \gamma_\mu P_L \ell_\beta)(\bar{f}'\gamma^\mu P f)\,, \tag{1.2}$$

where α, β are lepton flavor indices, f, f' are SM charged fermions and γ^μ are the Dirac gamma matrices. Here, P_L is the left-handed projection operator while P can be either P_L or P_R (the right-handed projection operator). These operators would lead to the so-called Non-Standard Interactions (NSI) in the neutrino sector [6–8] (for recent reviews, see [9, 10]). They are expected to arise generically from the exchange of some mediator state assumed to be heavier that the characteristic momentum transfer in the process. Operators in eq. (1.2) lead to the modification of neutrino production and detection mechanisms via new charged-current interactions (NSI-CC), while operators in eq. (1.1) induce new neutral-current processes (NSI-NC).

The operators in eq. (1.1) can modify the forward-coherent scattering (i.e., at zero momentum transfer) of neutrinos as they propagate through matter via so-called Mikheev-Smirnov-Wolfenstein (MSW) mechanism [6, 11]. Consequently their effect can be significantly enhanced in oscillation experiments where neutrinos travel large regions of matter, such as is the case for solar and atmospheric neutrinos. Indeed, the global analysis of data from oscillation experiments in the framework of mass induced oscillations in presence of NSI currently provides some of the strongest constraints on the size of the NSI affecting neutrino propagation [12, 13].

Curiously enough, the analysis from oscillation data still allows for a window into surprisingly large values of NSI couplings in the the so-called MSW LMA-Dark (LMA-D) [14] regime. For this solution, in contrast with the standard MSW LMA regime where the solar mixing angle is $\theta_{12} \approx 34°$, a value of this mixing angle in the 'dark' octant ($45° < \theta_{12} < 90°$) can fit solar and reactor data as long as large values of NSI are present, $\epsilon \sim \mathcal{O}(1)$ where ϵ relates the size of the new physics to the weak interaction. The origin of this solution is a degeneracy in oscillation data due to a symmetry of the Hamiltonian describing neutrino evolution in the presence of NSI [12, 13, 15, 16]. This degeneracy involves not only the octant of θ_{12} but also a change in sign of the larger neutrino mass-squared difference Δm^2_{31}, which is used to parameterize the type of neutrino mass ordering, normal versus inverted. Hence, the LMA-D degeneracy makes it impossible to determine the neutrino mass ordering by oscillation experiments [16], and therefore jeopardizes one of the main goals of the upcoming neutrino oscillation program. The only way to lift the degeneracy is by considering non-oscillation data to constrain NSI. One goal of this work is to investigate this possibility.

An alternative way to constrain operators in both eqs. (1.1) and (1.2) is through measurements of neutrino scattering cross sections with other fermions in the SM. For a compilation of bounds from scattering experiments on the size of NSI, see refs. [17–19] (notice however that in these studies usually only one NSI parameter is set to be different from

JHEP04(2017)116

zero at a time). Generically the "scattering" bounds on NSI-CC operators are presently rather stringent while the bounds on NSI-NC tend to be weaker. Still, in ref. [14] it was found that the combination of oscillation results with the NSI-NC scattering bounds could substantially lift the degeneracy between LMA and LMA-D, see also [20]. Nevertheless, a fully combined analysis of the oscillation data and the relevant results of scattering experiments is still missing in the literature. In particular, it is important to notice that the scattering cross section measurements are made in the deep-inelastic regime in which, at difference with the MSW effect in neutrino oscillations, a sizable momentum is transferred in the interaction.

A novel possibility to study the effect of the NSI operators in eq. (1.1) is through the measurement of coherent neutrino-nucleus scattering (CEνNS). Several experiments have been proposed for this task, e.g., at a stopped pion source [21] or at nuclear reactors [22–26]. In addition, solar neutrinos can in principle leave a signal in dark matter direct detection experiments [27].

In this work, we present the results of a global fit to vector-like NSI-NC operators, which are those that affect the flavor evolution of neutrinos in matter, using a combination of oscillation and scattering data. We will start by presenting the framework of our study in section 2. We will conclude that not all current constraints are applicable to all NSI models depending on the mass of the mediator and the momentum transfer in the interaction. Thus, in the following sections we will distinguish between two different classes of models, namely, NSI arising in models with heavy mediators, and NSI coming from models with light mediators (i.e., with masses much lighter than the electroweak scale). In both cases the bounds from oscillation experiments apply and we summarize them in section 3.1. The bounds from scattering experiments in the DIS regime only apply to models with heavy mediators. For those we describe our re-analysis of CHARM [28] and NuTeV [29] data, and the combination with oscillations in sections 3.2, 3.3, and 3.4, respectively. In section 4 we will consider the future sensitivity to NSI of a coherent neutrino-nucleus scattering experiment, and will take the COHERENT [21] proposal as an example. In this case, as in the case of oscillations, the bounds apply to all kind of models giving rise to NSI at low energies and we present the expected sensitivity when combined with the present constraints in section 5, focusing of the possibility to resolve the LMA-D degeneracy. We summarize our results and conclude in section 6. Analytical considerations related to the LMA-D degeneracy are presented in appendix A.

2 The NSI formalism

In this work, we will consider NSI affecting neutral-current (NC) processes relevant to neutrino propagation in matter. The coefficients accompanying the new operators are usually parametrized in the form:

$$\mathcal{L}_{\rm NSI} = -2\sqrt{2}G_F \sum_{f,P,\alpha,\beta} \epsilon^{f,P}_{\alpha\beta} (\bar{\nu}_\alpha \gamma^\mu P_L \nu_\beta)(\bar{f}\gamma_\mu P f)\,, \tag{2.1}$$

JHEP04(2017)116

where G_F is the Fermi constant, α, β are flavor indices, $P \equiv P_L, P_R$ and f is a SM charged fermion. In this notation, $\epsilon^f_{\alpha\beta}$ parametrizes the strength of the new interaction with respect to the Fermi constant, $\epsilon^f_{\alpha\beta} \sim \mathcal{O}(G_X/G_F)$.

2.1 NSI in neutrino oscillations and the LMA-D degeneracy

If all possible operators in eq. (2.1) are added to the SM Lagrangian, the Hamiltonian of the system which governs neutrino oscillations in presence of matter is modified as

$$H^\nu = H_{\rm vac} + H_{\rm mat} \equiv \frac{1}{2E} U_{\rm vac} \begin{pmatrix} 0 & & \\ & \Delta m^2_{21} & \\ & & \Delta m^2_{31} \end{pmatrix} U^\dagger_{\rm vac} + \sqrt{2} G_F N_e(x) \begin{pmatrix} 1+\epsilon_{ee} & \epsilon_{e\mu} & \epsilon_{e\tau} \\ \epsilon^*_{e\mu} & \epsilon_{\mu\mu} & \epsilon_{\mu\tau} \\ \epsilon^*_{e\tau} & \epsilon^*_{\mu\tau} & \epsilon_{\tau\tau} \end{pmatrix}, \tag{2.2}$$

where $U_{\rm vac}$ is the 3-lepton mixing matrix in vacuum [1, 3, 30]. $N_e(x)$ is the electron density as a function of the distance traveled by the neutrino in matter. For antineutrinos $H^{\bar\nu} = (H_{\rm vac} - H_{\rm mat})^*$. In eq. (2.2) the generalized matter potential depends on the "effective" NSI parameters $\epsilon_{\alpha\beta}$, defined as

$$\epsilon_{\alpha\beta} = \sum_{f=u,d,e} Y_f(x) \epsilon^{f,V}_{\alpha\beta} \,. \tag{2.3}$$

Note that the sum only extends to those fermions present in the background medium (up-quarks, down-quarks and electrons), and $Y_f(x) = N_f(x)/N_e(x)$ is the average ratio of the density for the fermion f to the density of electrons along the neutrino propagation path. In the Earth, the ratios Y_f are constant to very good approximation, while for solar neutrinos they depend on the distance to the center of the Sun. The presence of NSI with electrons, $f = e$, would affect not only neutrino propagation in matter as described in eq. (2.2), but also the neutrino-electron cross-section in experiments such as SK, Borexino, and reactor experiments. Since here we are only interested in studying the bounds to propagation effects in what follows we will consider only NSI with quarks. For feasibility reasons we restrict the analysis to the cases that NSI happen either for up quarks ($f = u$) or for down quarks ($f = d$).

In principle, the matter potential in eq. (2.2) contains a total of 9 additional parameters per f: three diagonal real parameters, and three off-diagonal complex parameters (i.e., 3 additional moduli and 3 complex phases). However, the evolution of the system given by the Hamiltonian in eq. (2.2) is invariant up to a constant. Therefore, oscillation experiments are only sensitive to the differences between the diagonal terms in the matter potential. In what follows, we choose to use the combinations $\epsilon_{ee} - \epsilon_{\mu\mu}$ and $\epsilon_{\tau\tau} - \epsilon_{\mu\mu}$. Also, it should be noted that only vector NSI ($\epsilon^V = \epsilon^L + \epsilon^R$) contribute to the matter potential in neutrino oscillations.

As a consequence of the CPT symmetry, neutrino evolution is invariant if the Hamiltonian in eq. (2.2) is transformed as $H^\nu \to -(H^\nu)^*$, see [12, 13] for a discussion in the context

JHEP04(2017)116

of NSI. This transformation can be realised by changing the oscillation parameters as

$$\begin{aligned} \Delta m^2_{31} &\to -\Delta m^2_{31} + \Delta m^2_{21} = -\Delta m^2_{32}\,, \\ \sin\theta_{12} &\to \cos\theta_{12}\,, \\ \delta &\to \pi - \delta\,, \end{aligned} \tag{2.4}$$

and simultaneously transforming the NSI parameters as

$$\begin{aligned} (\epsilon_{ee} - \epsilon_{\mu\mu}) &\to -(\epsilon_{ee} - \epsilon_{\mu\mu}) - 2\,, \\ (\epsilon_{\tau\tau} - \epsilon_{\mu\mu}) &\to -(\epsilon_{\tau\tau} - \epsilon_{\mu\mu})\,, \\ \epsilon_{\alpha\beta} &\to -\epsilon^*_{\alpha\beta} \quad (\alpha \neq \beta)\,, \end{aligned} \tag{2.5}$$

see refs. [13, 15, 16]. In eq. (2.4), δ is the leptonic Dirac CP phase, and we are using here the parameterization conventions from ref. [16]. In eq. (2.5) we take into account explicitly that oscillation data are only sensitive to differences in the diagonal elements of the Hamiltonian. Eq. (2.4) shows that this degeneracy implies a change in the octant of θ_{12} (as manifest in the LMA-D fit to solar neutrino data [14]) as well as a change in the neutrino mass ordering, i.e., the sign of Δm^2_{31}. For that reason it has been called "generalized mass ordering degeneracy" in ref. [16].

The $\epsilon_{\alpha\beta}$ in eq. (2.5) are defined in eq. (2.3) and depend on the density and composition of the medium. If NSI couple to quarks proportional to charge, $\epsilon^{u,V}_{\alpha\beta} = -2\epsilon^{d,V}_{\alpha\beta}$, they have the same dependence as the standard matter effect and the degeneracy is mathematically exact and no combination of oscillation experiments will be able to resolve it. In this work we consider only NSI with either up or down quarks and hence the degeneracy will be approximate, mostly due to the non-trivial neutron density along the neutrino path inside the Sun [13]. In particular, the first transformation in eq. (2.5) becomes

$$(\epsilon^{q,V}_{ee} - \epsilon^{q,V}_{\mu\mu}) \to -(\epsilon^{q,V}_{ee} - \epsilon^{q,V}_{\mu\mu}) - \xi_q \quad (q = u, d)\,, \tag{2.6}$$

where ξ_q depends on the effective matter composition relevant for the global data and will be determined from the fit.

2.2 Neutrino scattering and heavy versus light NSI mediators

Neutrino scattering experiments are sensitive to different combinations of $\epsilon^{f,P}_{\alpha\beta}$, depending on whether the scattering takes place with nuclei or electrons, the number of protons and neutrons in the target nuclei and other factors. In section 3 we will provide the combinations of parameters constrained by each experiment considered in our global fit.

Before proceeding with the combined analysis let us comment on the viability of renormalizable models leading to large coefficients in the neutrino sector. In particular it should be noted that the operators written in eq. (2.1) are not gauge invariant. Once gauge invariance is imposed to the full UV theory, the NSI operators listed above will be generated together with analogous operators in the charged lepton sector, which obey the same flavor structure. In this case, the non-observation of charge lepton flavor violating processes (CLFV) (e.g., $\mu \to eee$) imposes very tight constraints on the size of neutrino NSI for

JHEP04(2017)116

new physics above the electroweak (EW) scale. This eventually renders the effects of NSI unobservable at neutrino oscillation experiments, unless fine-tuned cancellations among operators with different dimensions are invoked to cancel the contributions to CLFV processes. This makes it extremely challenging to find a model of new physics above the EW scale that can lead to large NSI effects at low energies, see e.g., refs. [31–33].

An alternative, studied in some detail in refs. [34–38], is to assume that the neutrino NSI are generated by new physics well below the EW scale. For example, renormalizable, gauge-invariant models leading to large NSI have been constructed considering a Z' boson associated to a new $\mathrm{U}(1)_X$ symmetry, where X is a certain combination of lepton or baryon numbers. These models successfully avoid CLFV constraints through different mechanisms. Furthermore in these models the constraints coming from neutrino scattering data such as those from NuTeV [29] or CHARM experiments [28] can also be evaded. Generically the coupling times propagator of the Z' mediating neutrino scattering can be written as

$$\frac{g^2}{q^2 - M_{Z'}^2}\,, \tag{2.7}$$

where q is the momentum transfer in the process, and $M_{Z'}$ is the mass of the new vector boson. It is straightforward to see that, in the limit $q^2 \gg M_{Z'}^2$, the scattering amplitude will be roughly proportional to g^2/q^2, leading to a strong suppression of the effects in deep-inelastic scattering (DIS) experiments for sufficiently small couplings. Conversely, in neutrino oscillations, the potential felt by neutrinos in propagation through matter arises from forward coherent scattering, where the momentum transfer is zero, leading to effects proportional to $g^2/M_{Z'}^2$ instead.

Consequently in what follows we will distinguish between the bounds which apply to two different classes of NSI models:

1. models with *light* mediators, with masses from $\mathcal{O}(10\,\mathrm{MeV})$ to $\mathcal{O}(1\,\mathrm{GeV})$, and

2. models with *heavy* mediators, with masses from $\mathcal{O}(1\,\mathrm{GeV})$ to $\mathcal{O}(1\,\mathrm{TeV})$.

Those ranges are motivated by the typical energy scales of the scattering experiments considered below. To illustrate the potential of a future measurement of coherent neutrino-nucleus scattering we will consider the COHERENT proposal [21] based on a stopped pion source, providing neutrinos with energies less than about 50 MeV. The neutrino energies in the CHARM [28] and NuTeV [29] scattering experiments are $\gtrsim 10\,\mathrm{GeV}$. Hence, in the light mediator case COHERENT can test NSI, while effects in CHARM and NuTeV will be suppressed. Conversely, in the heavy mediator case all bounds would apply.

We do not consider mediators much heavier than $\mathcal{O}(1\,\mathrm{TeV})$ for the following reasons. Since we are interested mostly in $\epsilon \sim \mathcal{O}(1)$, mediators above the TeV scale would require large coupling constants violating perturbativity requirements. Moreover, in that case the contact-interaction approximation would hold even at LHC energies, and the corresponding operators would lead to missing energy signatures [39, 40]. A detailed investigation of this regime is beyond the scope of this work. Note that for the mediator mass ranges indicated above constraints from LHC derived under the contact-interaction assumption do not apply.

JHEP04(2017)116

3 Current experimental constraints

Current experimental constraints on vector-like NSI parameters include those obtained from a global fit to oscillation data [13], as well as those obtained from results from neutrino scattering data in the deep-inelastic regime. As mentioned above we will concentrate on NSI with either up or down quarks.[1] In this case the most precise scattering results are those from the CHARM [28] and NuTeV [29] experiments, which performed ν_e and ν_μ scattering on nuclei respectively. We present the details of our reanalysis of their results in sections 3.2 and 3.3 respectively. As discussed in the previous section we distinguish between NSI from models with light and heavy mediators. For light mediators, at present only the bounds from oscillations apply. The bounds for this scenario are summarized in section 3.1. For models with heavy mediators both, oscillation and scattering bounds apply and we present the combined bounds in section 3.4.

3.1 Oscillation experiments

For oscillation constraints on NSI parameters we refer to the comprehensive global fit in the framework of 3ν oscillation plus NSI with up and down quarks performed in [13] which we briefly summarize here for completeness. All oscillation experiments but SNO are only sensitive to vector NSI-NC via matter effects as described above. There is some sensitivity of SNO to axial couplings in their NC data. For this reason the analysis in ref. [13], and all combinations that we will present in what follows are made under the assumption of purely vector-like NSI.

The fit includes data sets from KamLAND reactor experiment [41] and solar neutrino data from Chlorine [42], Gallex/GNO [43], SAGE [44], Super-Kamiokande [45–48] Borexino [49, 50] and SNO [51–54], together with atmospheric neutrino results from Super-Kamiokande phases 1–4 [55], LBL results from MINOS [56, 57] and T2K [58], and reactor results from CHOOZ [59], Palo Verde [60], Double CHOOZ [61], Daya Bay [62] and RENO [63], together with reactor short baseline flux determination from Bugey [64, 65], ROVNO [66, 67], Krasnoyarsk [68, 69], ILL [70], Gösgen [71], and SRP [72].

In principle the analysis depends on the six 3ν oscillations parameters plus eight NSI parameters per f target, of which five are real and three are phases. To keep the fit manageable in ref. [13] only real NSI were considered and Δm^2_{21} effects were neglected in the analysis of atmospheric and LBL experiments. This renders the analysis independent of the CP phase in the leptonic mixing matrix. Furthermore in ref. [73] it was shown that strong cancellations in the oscillation of atmospheric neutrinos occur when two eigenvalues of $H_{\rm mat}$ are equal, and it is for this case that the weakest constraints are placed. This condition further reduces the parameter space to the 5 oscillation parameters plus 3 independent NSI parameters per f.

[1] This simplifying assumption should have little impact for the analysis of oscillation data. However, we note that once scattering data are included results may depend on the specific couplings to up and down quarks and, in particular, on whether both couplings are present simultaneously. A general analysis with arbitrary couplings is beyond the scope of this work and will be addressed in the future.

JHEP04(2017)116

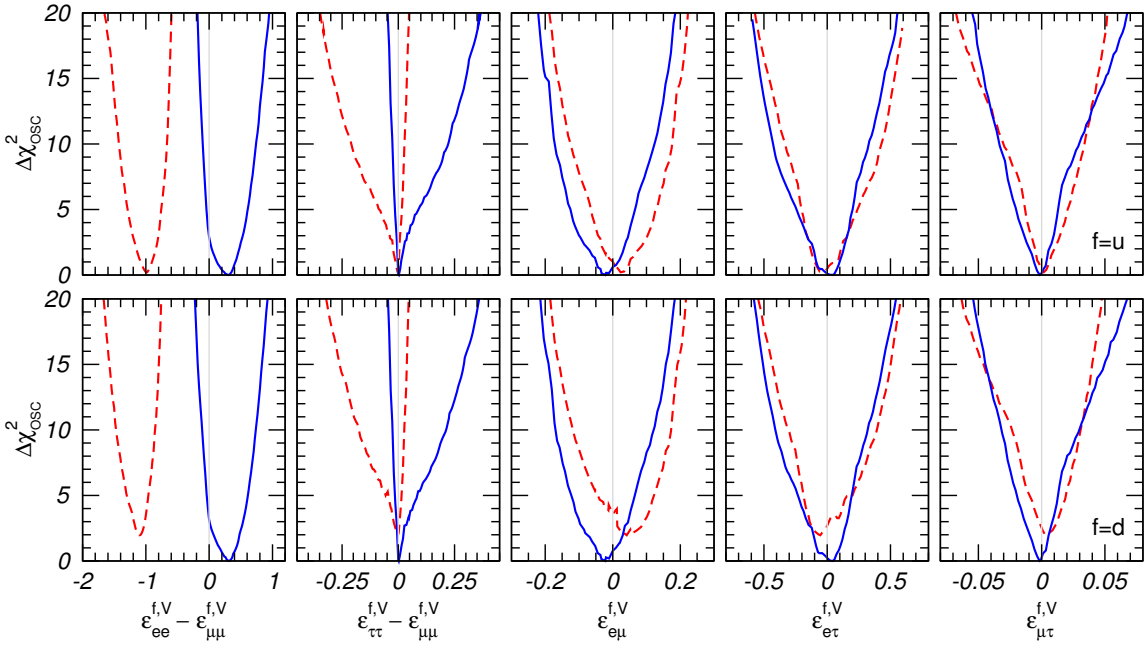

Figure 1. Dependence of the $\Delta\chi^2_{\rm OSC}$ function for the global analysis of solar, atmospheric, reactor and LBL data on the NSI parameters $\epsilon^{f,V}_{\alpha\beta}$ for $f = u$ (upper panels) and $f = d$ (lower panels). Solid curves correspond to the standard LMA solution and dashed curves correspond to the LMA-D degeneracy. These results correspond to the current limits assuming light NSI mediators. Results adopted from ref. [13].

We show in figure 1 the dependence of $\Delta\chi^2_{\rm OSC}$ on each of the relevant NSI coefficients obtained from the global analysis of oscillation data performed in ref. [13]. In each panel the results are shown after marginalization in the full parameter space of oscillation and considered NSI parameters. In the upper (lower) row these correspond to vector NSI with up (down) quarks, with all other NSI (i.e., NSI with electrons, axial, and vector ones with down (up) quarks) set to zero. In each row $\Delta\chi^2_{\rm OSC}$ is defined with respect to the global minimum in the corresponding parameter space. We also quote the corresponding allowed ranges at 90% CL in table 1.

When oscillation parameters are marginalized within the "standard" LMA region (solid curves in figure 1), the global oscillation analysis slightly favors non-vanishing diagonal NSI, with the best fit points $\epsilon^{f,V}_{ee} - \epsilon^{f,V}_{\mu\mu} = 0.307\,(0.316)$ for $f = u(d)$. The reason for this result is the 2σ tension in the determination of Δm^2_{21} in KamLAND and in Solar experiments (see, for example [4] for the latest status on this issue). This tension arises from two facts: i) neither SNO, SK, nor Borexino shows evidence of the low energy spectrum turn-up expected in the standard LMA-MSW solution for the value of Δm^2_{21} favored by KamLAND, and ii) the observation of a non-vanishing day-night asymmetry in SK, whose size is larger than the one predicted for the Δm^2_{21} value indicated of KamLAND. A small modification of the matter potential reduces this tension by $\Delta\chi^2 \sim 2$. The point of no NSI (all $\epsilon^{f,V}_{\alpha\beta} = 0$) has $\Delta\chi^2_{\rm OSC,min}$(no NSI) = 5.4 (same for up and down quarks) relative to the best fit, and is allowed at 63% CL (for the 5 additional NSI parameters).

JHEP04(2017)116

The dashed curves in figure 1 are obtained for the LMA-D degenerate solution [14], which correspond to the flipped mass spectrum according to eq. (2.4), including the second octant for θ_{12}. The dashed curves in the figure clearly follow the transformation from eq. (2.6), and comparing the LMA and LMA-D best fit points for $\epsilon_{ee}^{f,V} - \epsilon_{\mu\mu}^{f,V}$ we find

$$\xi_u = 0.685\,, \qquad \xi_d = 0.794\,. \tag{3.1}$$

Although the degeneracy is exact only for $\epsilon_{\alpha\beta}^{u,V} = -2\epsilon_{\alpha\beta}^{d,V}$, we see from the figure that it holds also to very good accuracy in the case of NSI with up or down quarks only. We find that for NSI with up-quarks (down-quarks) the LMA-D solution lies at a $\Delta\chi^2_{\rm OSC,min}(\text{LMA-D}) \simeq 0.2(1.9)$.

Since the oscillation results here summarized correspond to the analysis in ref. [13] they do not include data from oscillation experiments taken since fall 2013. As discussed above, the LMA-Dark solution emerges from a degeneracy in the oscillation probability and therefore the inclusion of that additional oscillation data would not have any quantitative impact relevant to the conclusions derived below in respect to the status of LMA-Dark. For the same reason, the LMA-Dark would appear in the analysis of oscillations if including NSI with general couplings to up and down quarks.

As mentioned above, these constraints from oscillations are presently the only constraints that apply to vector NSI with quarks for models with a mediator light enough to avoid the bounds from the deep-inelastic scattering experiments. Conversely for models with heavier mediators the constraints from DIS experiments apply as we describe next.

3.2 CHARM

The CHARM collaboration [28] measured the neutral- and charged-current ν_e and $\bar\nu_e$ cross sections with nuclei. To reduce the impact of systematic uncertainties, the ratio of the neutral-current (ν plus $\bar\nu$) to charged-current (ν plus $\bar\nu$) cross sections was reported [28]

$$R_e = \frac{\sigma(\nu_e N \to \nu_e X) + \sigma(\bar\nu_e N \to \bar\nu_e X)}{\sigma(\nu_e N \to e X) + \sigma(\bar\nu_e N \to \bar e X)} = 0.406 \pm 0.140\,, \tag{3.2}$$

which is related to the effective couplings $\tilde g_e^L$ and $\tilde g_e^R$ for electron neutrinos as

$$R_e = (\tilde g_e^L)^2 + (\tilde g_e^R)^2\,. \tag{3.3}$$

In presence of NSI, the effective couplings read

$$(\tilde g_e^P)^2 = \sum_{q=u,d} \left[(g_q^P + \epsilon_{ee}^{q,P})^2 + \sum_{\alpha\neq e} |\epsilon_{e\alpha}^{q,P}|^2 \right], \tag{3.4}$$

where g_q^P are the SM couplings of the Z boson to quarks, with tree-level values

$$\begin{aligned} g_u^L &= \frac{1}{2} - \frac{2}{3}\sin^2\theta_W\,, & g_u^R &= -\frac{2}{3}\sin^2\theta_W\,, \\ g_d^L &= -\frac{1}{2} + \frac{1}{3}\sin^2\theta_W\,, & g_d^R &= \frac{1}{3}\sin^2\theta_W\,. \end{aligned} \tag{3.5}$$

JHEP04(2017)116

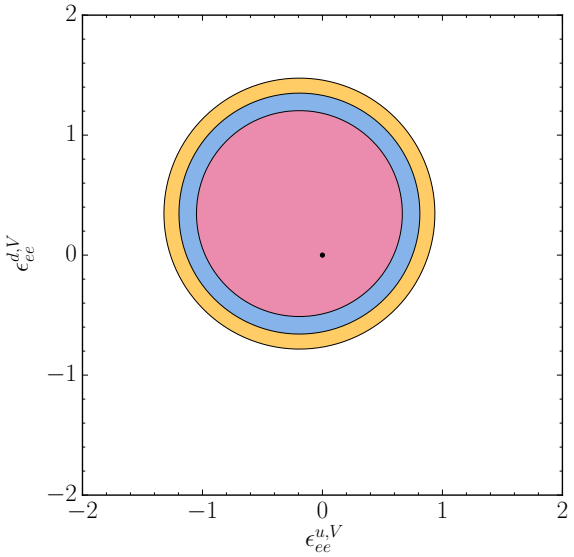

Figure 2. Allowed region from the CHARM measurement on two vector NSI parameters, $\epsilon_{ee}^{u,V}$ and $\epsilon_{ee}^{d,V}$ (for all other NSI couplings set to zero). The black dot shows the SM input value, while colored regions correspond to the $1, 2, 3\sigma$ contours for two degrees of freedom.

After including one-loop and leading two-loop radiative corrections [74], they take the values: $g_u^L = 0.3457$, $g_u^R = -0.1553$ $g_d^L = -0.4288$, and $g_d^R = 0.0777$ (so $R_{e,\mathrm{SM}} = 0.333$), where we have assumed a momentum transfer $Q^2 \sim 20\,\mathrm{GeV}^2$.

Using the constraint on R_e from eq. (3.2), we build the CHARM contribution to the χ^2 as

$$\chi^2_{\mathrm{CHARM}} = \left(\frac{R_{e,\mathrm{NSI}} - R_{e,\mathrm{CHARM}}}{\sigma_{\mathrm{CHARM}}} \right)^2 , \tag{3.6}$$

where $R_{e,\mathrm{NSI}}$ is taken from eq. (3.3), $R_{e,\mathrm{CHARM}} = 0.406$, and $\sigma_{\mathrm{CHARM}} = 0.140$. As illustration we show the bound from CHARM, projected onto the plane $(\epsilon_{ee}^{u,V}, \epsilon_{ee}^{d,V})$ in figure 2 setting all other NSI couplings to zero. From the figure we see that CHARM still allows for large $\epsilon_{ee}^{q,V}$. Also as the SM vector couplings are $g_q^V = g_q^L + g_q^R \simeq 0.19\,(-0.35)$ for up (down) quarks, the quadratic and linear contribution of the NSI to R_e have opposite signs for negative (positive) $\epsilon_{ee}^{u,V}$ $(\epsilon_{ee}^{d,V})$ and consequently the allowed region extends to larger negative (positive) values of the corresponding couplings.

3.3 NuTeV

NuTeV reported measurements of neutral-current (NC) and charged-current (CC) neutrino-nucleon scattering with both neutrinos and anti-neutrinos [29]. The ratios of NC to CC cross sections for either ν or $\bar{\nu}$ scattering from an isoscalar target can be written as

$$\begin{aligned} R_\mu^\nu &= \frac{\sigma_{\mathrm{NC}}(\nu_\mu)}{\sigma_{\mathrm{CC}}(\nu_\mu)} = (\tilde{g}_\mu^L)^2 + r(\tilde{g}_\mu^R)^2 , \\ R_\mu^{\bar{\nu}} &= \frac{\sigma_{\mathrm{NC}}(\bar{\nu}_\mu)}{\sigma_{\mathrm{CC}}(\bar{\nu}_\mu)} = (\tilde{g}_\mu^L)^2 + \frac{1}{r}(\tilde{g}_\mu^R)^2 , \end{aligned} \tag{3.7}$$

JHEP04(2017)116

with

$$r = \frac{\sigma_{\rm CC}(\bar{\nu}_\mu)}{\sigma_{\rm CC}(\nu_\mu)}\,. \tag{3.8}$$

In the presence of NSI, the effective couplings $\tilde{g}_\mu^L$ and $\tilde{g}_\mu^R$ get corrected as

$$g_{\rm eff}^P \equiv (\tilde{g}_\mu^P)^2 = \sum_{q=u,d}\left[(g_q^P + \epsilon_{\mu\mu}^{q,P})^2 + \sum_{\alpha\neq\mu}|\epsilon_{\mu\alpha}^{q,P}|^2\right], \tag{3.9}$$

where g_u^P and g_d^P are the SM couplings after including radiative corrections according to the momentum transfer in NuTeV. Their values can be extracted from the values for the SM effective couplings $g_{\rm eff,SM}^L$ and $g_{\rm eff,SM}^R$ given in refs. [29, 75], which include radiative corrections.

In order to reconstruct the ratios R_μ^ν and $R_\mu^{\bar{\nu}}$ the experiment classifies the events as NC or CC according to the event length topology. They report their results as ratios of short to long event rates in either ν or $\bar{\nu}$ beams [29]:

$$\begin{aligned} R_{\mu,\rm exp}^\nu &= 0.3916 \pm 0.00069\,({\rm stat}) \pm 0.00044\,({\rm sys}) \pm 0.0010\,({\rm mod}) = 0.3919 \pm 0.0013\,,\\ R_{\mu,\rm exp}^{\bar{\nu}} &= 0.4050 \pm 0.00159\,({\rm stat}) \pm 0.00057\,({\rm sys}) \pm 0.0021\,({\rm mod}) = 0.4050 \pm 0.0027\,, \end{aligned} \tag{3.10}$$

with an overall uncertainty correlation coefficient $\rho = 0.636$ [75]. The statistical error (stat), systematic error (sys) and theoretical errors associated to the model prediction (mod) are indicated separately for convenience.

The reconstructed experimental quantities in eq. (3.10) cannot be directly compared with the theoretical expression in eqs. (3.7) and (3.9) to obtain the constraints on the NSI, as the relation between the reconstructed short to long event rates and the cross section ratios in eq. (3.8) can only be determined using the Monte Carlo of the experiment. Instead, one can use the results of the experiment as given in terms of the fitted effective couplings [29, 75],

$$(g_{\rm eff,exp}^L)^2 = 0.30005 \pm 0.00137\,, \quad (g_{\rm eff,exp}^R)^2 = 0.03076 \pm 0.00110\,, \tag{3.11}$$

with overall uncertainty correlation coefficient $\rho = -0.017$. The NuTeV χ^2 function is then built as

$$\chi^2_{\rm NuTeV} = (\vec{X} - \vec{X}_{\rm exp})^t V_X^{-1} (\vec{X} - \vec{X}_{\rm exp})\,, \tag{3.12}$$

where

$$\vec{X} \equiv \begin{pmatrix} g_{\rm eff}^L \\ g_{\rm eff}^R \end{pmatrix}, \tag{3.13}$$

and

$$V_X = \begin{pmatrix} \sigma(g_{\rm eff,exp}^L)^2 & \sigma(g_{\rm eff,exp}^L)\,\sigma(g_{\rm eff,exp}^R)\,\rho \\ \sigma(g_{\rm eff,exp}^L)\,\sigma(g_{\rm eff,exp}^R)\,\rho & \sigma(g_{\rm eff,exp}^R)^2 \end{pmatrix}, \tag{3.14}$$

is the correlation matrix. Here, $\rho = -0.016$, $\sigma(g_{\rm eff,exp}^L) = 0.00137$ and $\sigma(g_{\rm eff,exp}^R) = 0.00110$ are taken from ref. [75]. Using this χ^2 implementation, one can easily see that the corresponding SM values for the effective couplings given in refs. [29, 75], $(g_{\rm eff,SM}^L)^2 = 0.3042$ and $(g_{\rm eff,SM}^R)^2 = 0.0301$, yield a $\chi^2_{\rm NuTeV,SM} \sim 9$. This is the well-known NuTeV anomaly.

JHEP04(2017)116

Since the publication of the NuTeV results, the requirement of several additional corrections to their analysis have been pointed out. Corrections related to nuclear effects, the fact that Fe is not an isoscalar target and the PDF of the strange quark among others [76, 77]. In ref. [77] a detailed evaluation of these effects found that all these corrections shift the central values of the R measurements by

$$\delta R^{\nu}_{\mu,\text{exp}} = 0.0017\,, \quad \delta R^{\bar{\nu}}_{\mu,\text{exp}} = -0.0016\,, \tag{3.15}$$

where $\delta R_{\mu,\text{exp}} \equiv R_{\mu,\text{exp corr}} - R_{\mu,\text{exp orig}}$. To translate these shifts into shifts of the effective couplings we follow the procedure employed by the collaboration in their fit to the effective couplings by using the Jacobian J of the transformation between the two sets of variables, $\delta\vec{X} = J^{-1}\delta\vec{R}$. The Jacobian is determined by the experimental collaboration via Monte Carlo simulation. Its value can be found in [75].

With this we get that the results in eq. (3.11) get shifted as

$$\delta g^{L}_{\text{eff,exp}} = 0.00242\,, \quad \delta g^{R}_{\text{eff,exp}} = -0.00155\,, \tag{3.16}$$

which bring the corrected experimental results to reasonable agreement with the SM expectations, $\chi^2_{\text{NuTeV,SM}} \sim 2.3$.

We adopt these corrected experimental effective coupling results to derive the corresponding constraints on the NSI, using the expectations in eq. (3.9) with radiative-corrected SM couplings for the up and down quarks $g^L_u = 0.3493$, $g^R_u = -0.1551$ $g^L_d = -0.4269$, and $g^R_d = 0.0776$ (which correctly reproduce the SM predicted values of $(g^P_{\text{eff,SM}})^2$ given by the collaboration). As illustration, in figure 3 we show the bound from NuTeV in the plane of the couplings g^L_{eff} and g^R_{eff} (left panel), as well as in the plane $(\epsilon^{u,V}_{\mu\mu}\,, \epsilon^{d,V}_{\mu\mu})$ (right panel).

3.4 Global fit to current experiments — heavy NSI mediators

With the results above we can now proceed to performed a combined analysis of the oscillation and scattering experiments by constructing

$$\chi^2_{\text{OSC+SCAT}} \equiv \chi^2_{\text{OSC}} + \chi^2_{\text{CHARM}} + \chi^2_{\text{NuTeV}}\,, \tag{3.17}$$

and to constrain the vector-like NSI (assuming vanishing axial couplings) with quarks. These are the present bounds relevant for models with heavy mediators (as defined in section 2.2). In order to keep the analysis feasible, we will consider real NSI parameters. In all cases, we will show our results as $\Delta\chi^2 \equiv \chi^2 - \chi^2_{\text{min}}$, where χ^2_{min} is the global minimum of the χ^2.

We show in figure 4 the dependence of $\Delta\chi^2_{\text{OSC+SCAT}}$ on each of the relevant NSI coefficients (after marginalizing over all oscillation and NSI undisplayed parameters) for interactions with either up or down quarks. We also quote the corresponding allowed ranges at 90% CL in table 1. From the figure we see how the inclusion of the results from the scattering experiments resolves the degeneracy for the flavor-diagonal NSI parameters

JHEP04(2017)116

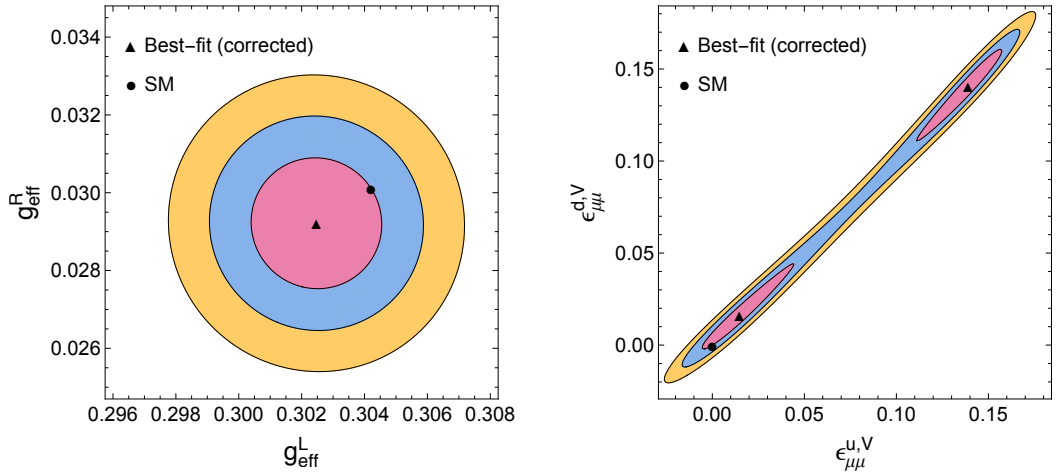

Figure 3. Allowed regions obtained from the NuTeV measurement. Contours correspond to 1σ, 2σ and 3σ for 2 degrees of freedom. The triangle indicates the best-fit points, which are completely degenerate. The SM (indicated by a dot) is allowed at $\sim 1\sigma$. The left panel shows allowed regions in the plane of the couplings $g^L_{\rm eff}$ and $g^R_{\rm eff}$. The right panel shows the region obtained for the two vector NSI parameters $\epsilon^{u,V}_{\mu\mu}$ and $\epsilon^{d,V}_{\mu\mu}$, after setting all other NSI parameters set to zero.

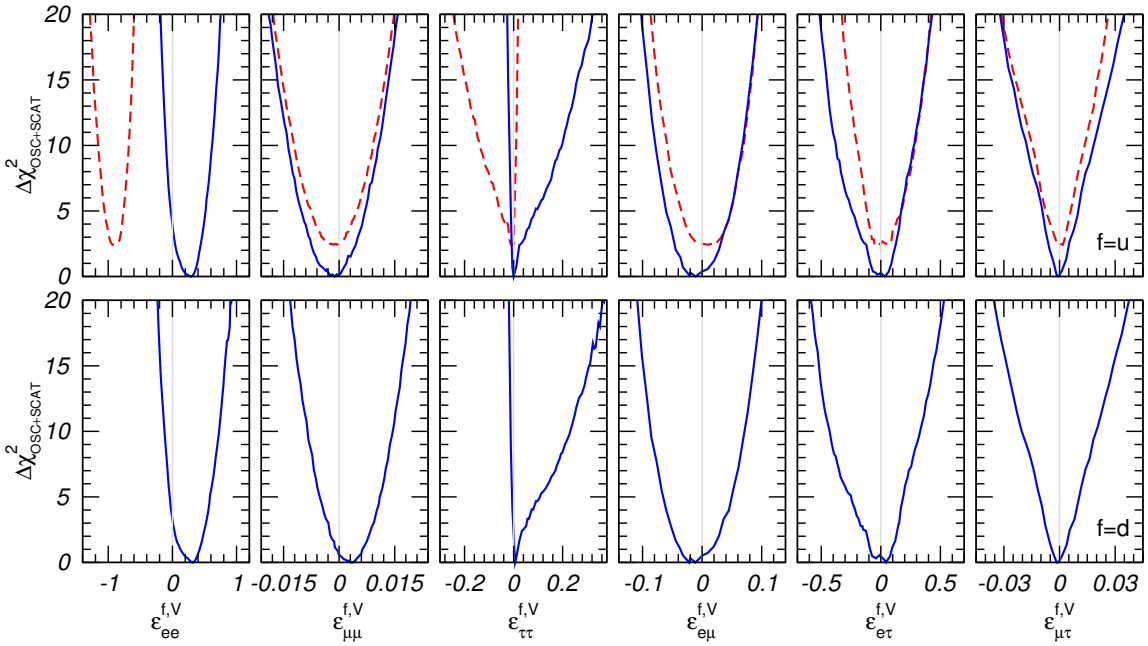

Figure 4. Dependence of the $\Delta\chi^2_{\rm OSC+SCAT}$ on the NSI parameters $\epsilon^{q,V}_{\alpha\beta}$ for $q = u$ (upper panels) and $q = d$ (lower panels), for both LMA (solid) and LMA-D (dashed) regions from the combined analysis of global oscillation and CHARM + NuTeV scattering data. These results correspond to the current limits assuming heavy NSI mediators.

JHEP04(2017)116

from oscillations. This results in very strong bounds in the $\epsilon^{q,V}_{\mu\mu}$ direction, driven mostly by NuTeV.[2]

For NSI with down-quarks the LMA-D degeneracy becomes disfavored at more than 5σ, in agreement with the the results from ref. [14]; specifically for this case we have $\Delta\chi^2_{\rm OSC+SCAT,min}(\text{LMA-D}) = 27$. However, our results show that for NSI with up-quarks the LMA-D solution is still allowed at 1.5σ ($\Delta\chi^2_{\rm OSC+SCAT,min}(\text{LMA-D}) = 2.4$). The difference between the results for LMA-D for up and down quarks can be easily understood as follows: LMA-D requires $\epsilon^{q,V}_{ee} - \epsilon^{q,V}_{\mu\mu} \sim \mathcal{O}(-1)$ which given the constraints on $\epsilon^{q,V}_{\mu\mu}$ for either $q = u$ or d imposed by NuTeV (see figure 3), implies that $\epsilon^{q,V}_{ee} \sim \mathcal{O}(-1)$, a value ruled out by CHARM for $q = d$ but still allow for $q = u$ as seen in figure 2.

4 A future experiment on coherent neutrino-nucleus scattering

As mentioned in section 2, the bounds derived from NuTeV and CHARM are not applicable to NSI models with light mediators. In this case, it would be necessary to include constraints from scattering experiments with low momentum transfer, in addition to those from oscillations to constrain all the NSI parameters. Neutrino-nucleus coherent scattering experiments can be used for this purpose [78–81]. Several proposals have been envisaged for the future, which can be divided in two different categories, according to their neutrino source: those using nuclear reactors (e.g., TEXONO [22], CONNIE [23, 24], MINER [25], or at the Chooz reactor [26]), and those using a stopped pion source (COHERENT [21]). An important difference between the two approaches is the flavor composition of the source. A reactors emits only electron anti-neutrinos and hence we can test only NSI parameters $\epsilon_{e\alpha}$ ($\alpha = e, \mu, \tau$). The stopped pion source provides neutrinos of muon and electron flavor which to some extent can be disentangled by using timing information, as we explain in more detail below. Hence, there we can constrain both, $\epsilon_{e\alpha}$ and $\epsilon_{\mu\alpha}$. To be specific, we will consider in this work the COHERENT proposal [21] as an example for a coherent neutrino-nucleon scattering experiment at a stopped pion source, and comment on how the results would change in case of a reactor measurement. For recent sensitivity investigations of a reactor based experiment see refs. [80, 81].

COHERENT will place several low threshold detectors located within tens of meters from the Spallation Neutrino Source (SNS) [82] at Oak Ridge National Laboratory. A variety of nuclear targets have been considered, including CsI, NaI, Ge, Ne and Ar. The combination of different phases using different nuclear targets would be beneficial not only because of the increase in statistics, but also because it would allow to study the dependence of the signal with Z and N (see eq. (4.3)). In this work, for simplicity, we will only consider a ^{76}Ge detector, located at a distance of 22 m from the source. We will assume a detection threshold of 5 keV for nuclear recoils and a nominal exposure of 10 kg·yrs, following refs. [21, 83]. In order to illustrate the effect on the results of combining

[2]Note that this strong constraint follows from our assumption of interactions either with up or down quarks. As visible in figure 3 there is a strong correlation of $\epsilon^{u,V}_{\mu\mu}$ and $\epsilon^{d,V}_{\mu\mu}$. In the direction $\epsilon^{u,V}_{\mu\mu} \approx \epsilon^{d,V}_{\mu\mu}$ the NuTeV constraint is much weaker and values up to $\epsilon^{u,V}_{\mu\mu} \approx \epsilon^{d,V}_{\mu\mu} \approx 0.18$ are allowed by NuTeV. In fact, the two minima shown in figure 3 are completely degenerate.

JHEP04(2017)116

data taken using different nuclei, for some of the results shown in section 5 we will also add a second detector with a Ne target.

At the SNS, the main component of the flux will be a monochromatic ν_μ line coming from $\pi^+ \to \mu^+ \nu_\mu$. Subleading contributions to the flux come from the subsequent decays $\mu^+ \to e^+ \bar{\nu}_\mu \nu_e$ (thus $|\vec{p}_\mu| = E_{\nu_\mu} = (m_\pi^2 - m_\mu^2)/2/m_\pi = 30\,\text{MeV}$). So the the energy distributions (normalized to 1) for each neutrino flavor at the source can be obtained from simple decay kinematics (neglecting the small μ momentum, ie taking the muon at rest also), as

$$\begin{aligned} f_{\nu_\mu} &= \delta\left(E_\nu - \frac{m_\pi^2 - m_\mu^2}{2m_\pi}\right), \\ f_{\bar{\nu}_\mu} &= \frac{64}{m_\mu}\left[\left(\frac{E_\nu}{m_\mu}\right)^2\left(\frac{3}{4} - \frac{E_\nu}{m_\mu}\right)\right], \\ f_{\nu_e} &= \frac{192}{m_\mu}\left[\left(\frac{E_\nu}{m_\mu}\right)^2\left(\frac{1}{2} - \frac{E_\nu}{m_\mu}\right)\right], \end{aligned} \tag{4.1}$$

where $E_\nu \in [0, m_\mu/2]$ is the energy of the resulting neutrino, m_π is the pion mass and m_μ is the muon mass. As seen from eq. (4.1), the monochromatic ν_μ flux line has an energy of $\sim 30\,\text{MeV}$, while the two other contributions will have a continuous spectrum until they reach the end point of the decay at around 50 MeV. The total flux $\phi(E_\alpha)$ is obtained multiplying the distributions in eq. (4.1) by an overall normalization factor, determined by the total number of protons on target and the number of pions produced per incident proton. We set this normalization constant following ref. [79], so that the total neutrino flux entering the detector is 10^7 neutrinos per second.

The coherent interaction cross section for a given neutrino flavor α, in presence of neutral-current NSI, can be written as

$$\frac{d\sigma_\alpha}{dE_r} = \frac{G_F^2}{2\pi}\frac{Q_{w\alpha}^2}{4}F^2(2ME_r)M\left(2 - \frac{ME_r}{E_\nu^2}\right), \tag{4.2}$$

where E_r is the nuclear recoil energy, $F(Q^2)$ is the nuclear form factor (taken from ref. [84]), M is the mass of the target nucleus and E_ν is the incident neutrino energy. We have defined $Q_{\omega\alpha}^2$ as

$$\begin{aligned} \frac{1}{4}Q_{w\alpha}^2 = &\left[Z(g_p^V + 2\epsilon_{\alpha\alpha}^{u,V} + \epsilon_{\alpha\alpha}^{d,V}) + N(g_n^V + \epsilon_{\alpha\alpha}^{u,V} + 2\epsilon_{\alpha\alpha}^{d,V})\right]^2 \\ &+ \sum_{\beta\neq\alpha}\left[Z(2\epsilon_{\alpha\beta}^{u,V} + \epsilon_{\alpha\beta}^{d,V}) + N(\epsilon_{\alpha\beta}^{u,V} + 2\epsilon_{\alpha\beta}^{d,V})\right]^2. \end{aligned} \tag{4.3}$$

Here, N and Z are the number of neutrons and protons in the target nucleus ($Z = 32$ and $N = 44$ for ^{76}Ge), respectively, while $g_p^V = \frac{1}{2} - 2\sin^2\theta_W$, $g_n^V = -\frac{1}{2}$ are the SM couplings to the Z boson to protons and neutrons, θ_W being the weak mixing angle.

The differential event distribution for a given flavor is obtained from the convolution of the neutrino flux and cross section, multiplying by appropriate normalization factors to account for the total luminosity of the experiment. The result can be expressed as

$$\frac{dN_\alpha}{dE_r} = N_t\Delta t\int dE_\nu \phi_\alpha(E_\nu)\frac{d\sigma_\alpha}{dE_r}(E_\nu), \tag{4.4}$$

JHEP04(2017)116

where N_t is the number of nuclei in the detector, and Δt is the considered data taking period. In the absence of a detailed publicly available simulation of the expected performance of the COHERENT detector, we will assume perfect detection efficiency[3] and will use no spectral information in our analysis (only the total event rates, as explained below). The total number of events is obtained after integrating eq. (4.4) over E_r above detection threshold.

We will apply a timing cut to separate the prompt signal (which comes mainly from the monoenergetic ν_μ's) from the delayed signal (which comes mainly from the decay products of the muon). This separation however is not perfect. Considering that the muon lifetime from a stopped pion is $\Gamma\tau = 2.283\ \mu$s, and that the SNS proton pulses are relatively wide ($t_w = 0.695\,\mu$s) [82], there is a certain probability for a muon to decay within the duration of a given pulse. In this case, the neutrinos produced from the muon decay may contaminate the prompt signal window with a probability

$$P_c = \frac{1}{t_w}\int_0^{t_w} dt\left[1 - e^{-(t_w - t)/\Gamma\tau}\right] = 0.138\,, \tag{4.5}$$

where we have assumed a flat pulse shape. We have explictly checked that the allowed values of NSI are hardly affected by this assumption or even by modifications leading to changes of P_c by factors $\mathcal{O}$(few). The number of events detected within the prompt (N_p) and delayed (N_d) time windows are thus given by

$$\begin{aligned} N_p &= N_{\nu_\mu} + P_c(N_{\nu_e} + N_{\bar{\nu}_\mu})\,, \\ N_d &= (1 - P_c)(N_{\nu_e} + N_{\bar{\nu}_\mu})\,. \end{aligned} \tag{4.6}$$

For the main configuration considered in this work, that is, a ^{76}Ge detector with a 5 keV threshold and a nominal exposure of 10 kg·yr, we obtain approximately 113 (200) events in the prompt (delayed) window. These numbers are in good agreement with ref. [79].

The experiment will be subject to systematic uncertainties affecting the beam flux normalization, detector performance, etc. Following ref. [79], we estimate prior uncertainties to be at the 10% level. Significant backgrounds are expected from two main sources: (1) beam-related backgrounds, especially fast neutrons which enter the detector, and (2) backgrounds from cosmic ray interactions and radioactivity. Based on ref. [21], we estimate the number of background events to be approximately 20% of the number of signal events. We include them in our chi-square implementation using the pull method, assuming they contribute to the statistical error of the measurement.

Given that the expected statistics is in the range of a few hundred of events per bin, a Gaussian χ^2 is used for the COHERENT experiment,

$$\chi^2_{\rm COH} = \min_{\xi} \sum_{k=p,d} \left(\frac{(1+\xi)N_{k,\rm NSI} - N_{k,\rm obs}}{\sqrt{N_{k,\rm obs} + 0.2N_{k,\rm obs}}}\right)^2 + \left(\frac{\xi}{\sigma_{\rm sys}}\right)^2\,, \tag{4.7}$$

where $\sigma_{\rm sys} = 0.1$ as explained above, and the result is minimized over the nuisance parameter ξ associated to the signal normalization. Here, $N_{p,\rm obs}$ and $N_{d,\rm obs}$ denote the simulated

[3] A lower detection efficiency can be easily corrected for by increasing the total exposure over the nominal value.

JHEP04(2017)116

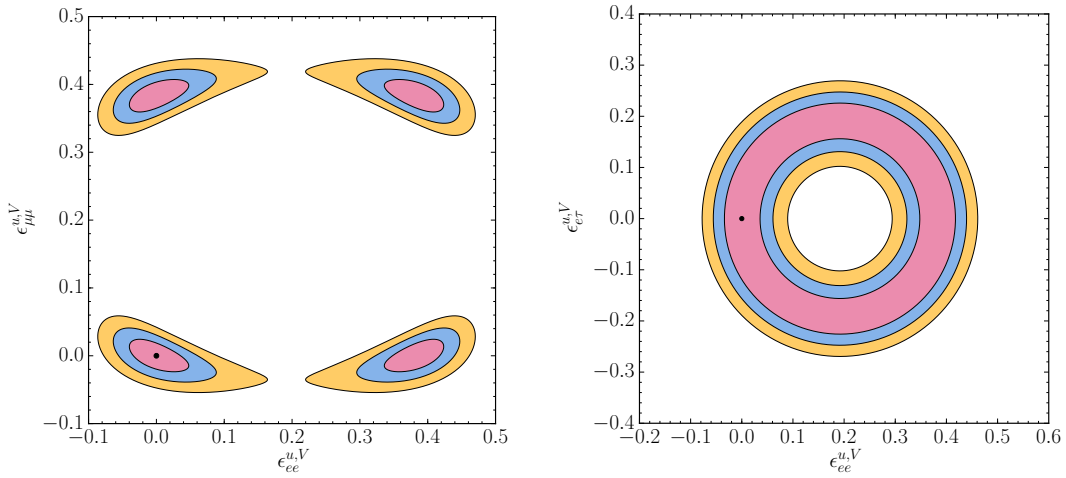

Figure 5. The projected COHERENT sensitivity to NC vector-like NSI parameters. The left (right) panel shows the expected confidence regions projected onto the $\epsilon^{u,V}_{ee} - \epsilon^{u,V}_{\mu\mu}$ ($\epsilon^{u,V}_{ee} - \epsilon^{u,V}_{e\tau}$) plane, after setting the remaining NSI parameters to zero. In both cases, the pink, blue and yellow regions indicate the allowed regions at 1σ, 2σ and 3σ (for 2 d.o.f.). The black dots indicate the SM, which has been used to generate the simulated experimental data used in this figure. The experiment has been simulated using 10 kg·yr exposure for ^{76}Ge, see section 4 for details.

data that we assume the experiment will observe in the prompt and delayed time windows, respectively, while the corresponding expected values in presence of NSI parameters are denoted as $N_{p,\mathrm{NSI}}$ and $N_{d,\mathrm{NSI}}$.

Figure 5 shows the expected sensitivity for the COHERENT setup, simulated as described above, to several NSI parameters affecting neutrino interactions with up quarks (the corresponding regions for interactions with down quarks are very similar). In both panels, SM interactions (i.e., zero NSI) have been assumed to simulate the COHERENT "observed" data, and the result is fitted allowing for the presence of NSI. All NSI parameters not shown in each panel have been set to zero for simplicity in this figure; in the results shown in the next section, however, they are all included and the chi-squared is minimized over all parameters not shown.

A coherent scattering experiment at a reactor would be sensitive only to the NSI combination Q^2_{we}, as defined in eq. (4.3). Hence we would obtain a qualitatively similar behavior of the NSI sector involving the electron flavor (for instance as shown in the right panel of figure 5). In contrast to the configuration shown in the left panel, there would be no sensitivity to $\epsilon^{q,V}_{\mu\mu}$ from a reactor experiment. This will turn out to be crucial for resolving the LMA-D degeneracy, as we will discuss below.

5 Expected combined sensitivity after inclusion of COHERENT

In this section we add to our global fit the expected results for the COHERENT experiment. As before, we consider two scenarios depending on the assumed mass range of the mediator responsible for the NSI. In all cases, we will show our results as $\Delta\chi^2 \equiv \chi^2 - \chi^2_{\mathrm{min}}$, where

JHEP04(2017)116

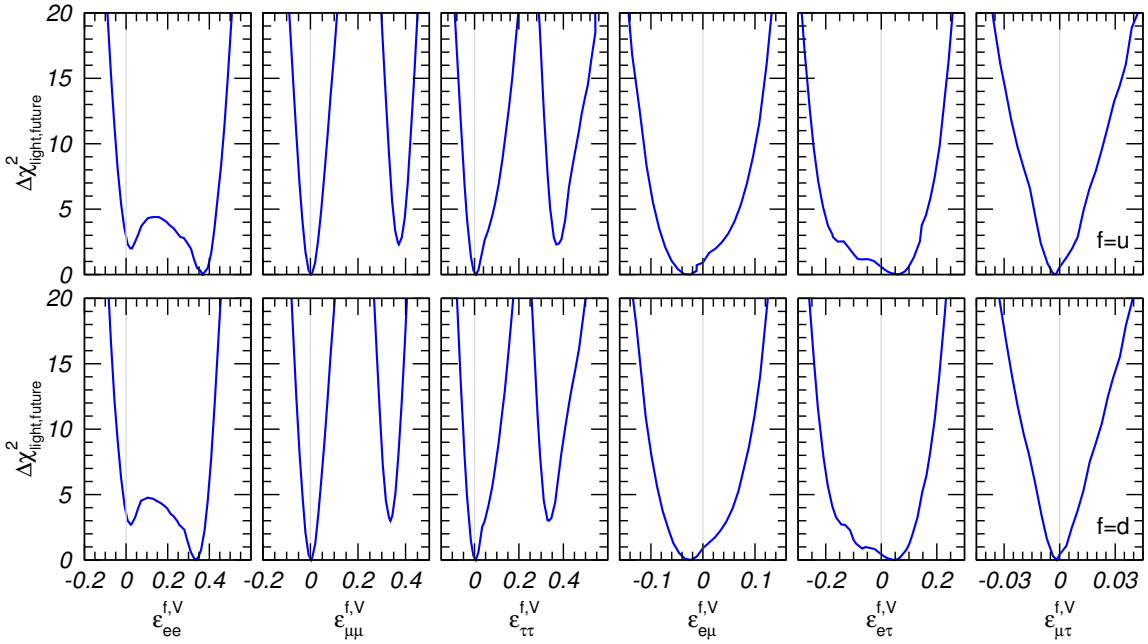

Figure 6. Dependence of $\Delta\chi^2_{\text{light,future}}$ on the NSI parameters $\epsilon^{f,V}_{\alpha\beta}$ for $f = u$ (upper panels) and $f = d$ (lower panels), using current global data on oscillations combined with artificial COHERENT data generated for all $\epsilon_{\alpha\beta}$ set to zero.

χ^2_{min} is the global minimum of the χ^2. The particular combination of experiments included in the χ^2 will depend on the scenario being considered, as described in more detail below. As before, we will consider real NSI and will assume vanishing axial NSI couplings.

5.1 NSI from a light mediator

As explained in section 2, if NSI are produced from new interactions with a light mediator the only applicable bounds are those obtained from experiments with small momentum transfer, i.e., those derived from oscillation data and COHERENT. Therefore in this case we construct our combined chi-squared function as

$$\chi^2_{\text{light,future}} = \chi^2_{\text{OSC}} + \chi^2_{\text{COH}} \,. \tag{5.1}$$

In the case of oscillations, we will use the results from the global fit performed in ref. [13]. In the case of COHERENT, some assumption needs to be made regarding the "true" values of the NSI parameters which will be used as input to generate the simulated data. A natural possibility would be to set all ϵ to zero. A second possibility would be to use the best-fit from oscillation data, which shows a slight preference for non-zero NSI. We will consider those two cases below.

Figure 6 shows the results for the combination of oscillation data, plus COHERENT data simulated for vanishing NSI coefficients. In generating these results we have assumed our template COHERENT configuration of 10 kg·yrs of ^{76}Ge with a threshold of 5 keV for nuclear recoils, see section 4 for details. The results are shown for the NSI coefficients

JHEP04(2017)116

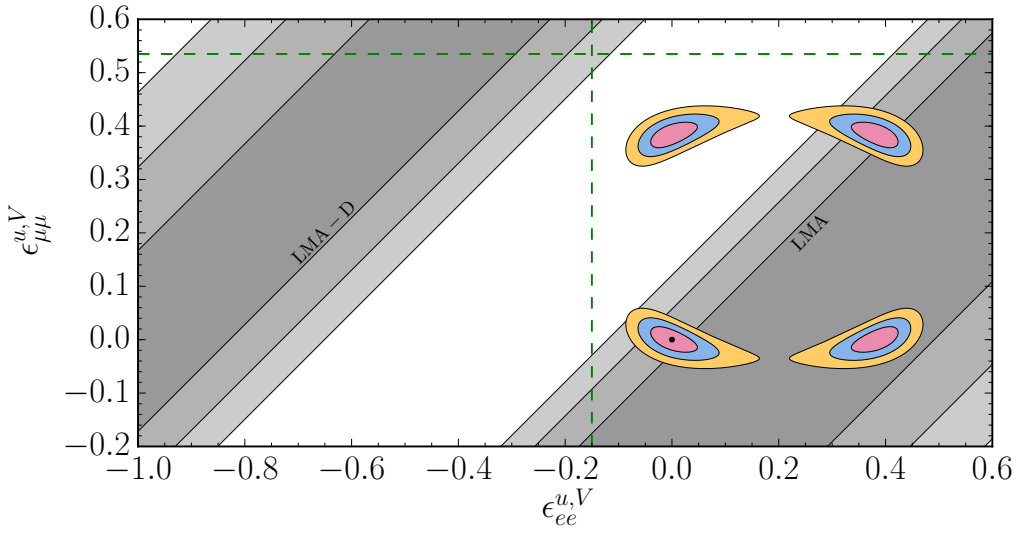

Figure 7. Allowed regions in the plane of $\epsilon_{ee}^{u,V}$ and $\epsilon_{\mu\mu}^{u,V}$ from the COHERENT experiment (under the assumption of no NSI in the data — same as in figure 5) overlayed with the presently allowed regions from the global oscillation analysis. The two diagonal shaded bands correspond to the LMA and LMA-D regions as indicated, at 1, 2, 3σ. The dashed lines indicate the values of NSI parameters for which COHERENT would not be able to resolve the LMA-D degeneracy, see appendix A for details.

assuming that the new interactions take place with either up or down quarks, as indicated by the labels in each row. As mentioned earlier, we include all NSI parameters at once in the fit. Thus, in each panel, the results have been obtained after marginalization over all parameters not shown, including standard oscillation parameters and NSI parameters. For this configuration we find that the LMA-D solution can be ruled out (for NSI with up or with down quarks) at high CL. In particular we obtain $\Delta\chi^2_{\text{light,future}}(\text{LMA-D}) > 45\,(80)$ for NSI with up (down) quarks. This is obvious from figure 7, where we show the allowed regions in the plane of $\epsilon_{ee}^{u,V}$ and $\epsilon_{\mu\mu}^{u,V}$ from oscillations together with the 4 degenerate solutions from COHERENT (same as in figure 5). The regions from oscillations are diagonal bands in this plane, since oscillations determine only the difference $\epsilon_{ee}^{u,V} - \epsilon_{\mu\mu}^{u,V}$. We see that the band corresponding to the LMA-D region is far away from the COHERENT solutions and can therefore be excluded by the combination. Consequently, in figure 6 only the results obtained for the LMA solution appear. The corresponding allowed ranges at 90% CL are reported in table 1.

For the LMA solution, comparing to the present bounds from oscillations (see figure 4), we see that no significant improvement is expected in the determination of the flavor-changing NSI parameters. The main impact of COHERENT is in the determination of the flavor diagonal ones: as it provides information on $\epsilon_{ee}^{q,V}$ and $\epsilon_{\mu\mu}^{q,V}$, the combination with oscillations allows for the independent determination of the three flavor-diagonal couplings. However, three minima still remain for the combined chi-squared, one global and two quasi-degenerate local. This is explained as follows. First, COHERENT is completely insensitive

JHEP04(2017)116

to $\epsilon^{f,V}_{\tau\tau}$, as shown in eq. (4.3). This means that $\epsilon^{f,V}_{\mu\mu}$ can be different from zero, as long as $\epsilon^{f,V}_{\tau\tau}$ is set accordingly in order to respect the bounds from oscillations, which constrain $\epsilon^{f,V}_{\tau\tau} - \epsilon^{f,V}_{\mu\mu} \approx 0$. Second, the shape of $\chi^2_{\rm COH}$, as shown in figure 5, has four separate minima in the plane of $\epsilon^{f,V}_{ee}$ and $\epsilon^{f,V}_{\mu\mu}$. As can be seen from figure 7, the position of the low right region matches very well the allowed values from oscillation data for the LMA case $\epsilon^{f,V}_{ee} - \epsilon^{f,V}_{\mu\mu} \approx 0.3$. This leads to the global minimum observed in the one dimensional projection of the combined $\Delta\chi^2_{\rm light,,future}$ for $\epsilon^{f,V}_{ee} \approx 0.35$ and $\epsilon^{f,V}_{\mu\mu} \simeq \epsilon^{f,V}_{\tau\tau} \approx 0$, see figure 6. In addition, there are two other sets of NSI for which local minima are found in the multi-dimensional parameter space. In the $(\epsilon^{f,V}_{ee}, \epsilon^{f,V}_{\mu\mu})$ plane shown in figure 7 they correspond to the lower left and upper right COHERENT regions. Combined with the oscillation constraint $\epsilon^{f,V}_{\tau\tau} - \epsilon^{f,V}_{\mu\mu} \approx 0$, the first set corresponds to $\epsilon^{f,V}_{ee} \simeq \epsilon^{f,V}_{\mu\mu} \simeq \epsilon^{f,V}_{\tau\tau} = 0$, which is visible as the local minimum in the first panel in figure 6. The second set corresponds to $\epsilon^{f,V}_{ee} \simeq \epsilon^{f,V}_{\mu\mu} \simeq \epsilon^{f,V}_{\tau\tau} = 0.3$ which appears as the local minimum in the second and third panels of figure 6. In both cases the oscillation probability has no flavor-diagonal NSI effects and yields about the same $\Delta\chi^2_{\rm OSC} \simeq 2$ (see first panel in figure 1).

Let us now relax the assumption that the true values of the NSI parameters are zero. To generate COHERENT data we adopt now the best fit point obtained in the oscillation analysis for light mediators, see section 3.1. However, since oscillations are sensitive only to the differences of flavor-diagonal NSI, one of the $\epsilon^{q,V}_{\alpha\alpha}$ remains undetermined and can be chosen arbitrarily. We use $\epsilon^{q,V}_{ee,\rm true}$ as independent diagonal parameter. We can now perform the combined oscillation+COHERENT fit, by scanning the value of $\epsilon^{q,V}_{ee,\rm true}$, and all other NSI parameters assumed to generate COHERENT data are determined by the best fit point from oscillations (in particular, also the other two diagonal parameters $\epsilon^{q,V}_{\mu\mu,\rm true}$ and $\epsilon^{q,V}_{\tau\tau,\rm true}$).

Let us focus on the question of whether the LMA-D degeneracy can be lifted by the combination of oscillation and COHERENT data if $\epsilon^{q,V}_{ee,\rm true}$ is allowed to take on arbitrary values. The full red curve in figure 8 shows the $\Delta\chi^2_{\rm min}$ of the LMA-D region as a function of $\epsilon^{q,V}_{ee,\rm true}$ for our default COHERENT configuration (^{76}Ge detector with 5 keV threshold, 10 kg·yrs, and 10% normalization systematics). We find that there are two local minima of this curve, which means that there are certain values of $\epsilon^{q,V}_{ee,\rm true}$ for which the combination of oscillation and COHERENT data will not be able to resolve the LMA-D degeneracy. The location of the minima can be understood analytically from the combinations of NSI parameters which COHERENT is sensitive to according to eq. (4.3). We provide the relevant equations in appendix A. The values of $\epsilon^{q,V}_{ee}$ and $\epsilon^{q,V}_{\mu\mu}$ for which COHERENT cannot resolve the degeneracy are shown as dashed lines in figure 7. The region where they cross the allowed band from LMA corresponds to the location of the minima in figure 8. In those locations COHERENT is completely blind to the degeneracy and the χ^2 seen in the figure is just the one present already in the oscillation-only analysis. Moreover, the figure shows that there is a relevant region of the parameter space around those minima, where the LMA-D degeneracy would remain at low CL. Also as seen in the figure, reducing the normalization systematics in COHERENT to 1% (dashed red line) has a negligible impact.

However, if Nature happens to chose parameter values close to those points, the oscillation+COHERENT combination will be able to establish the existence of NSI at very

JHEP04(2017)116

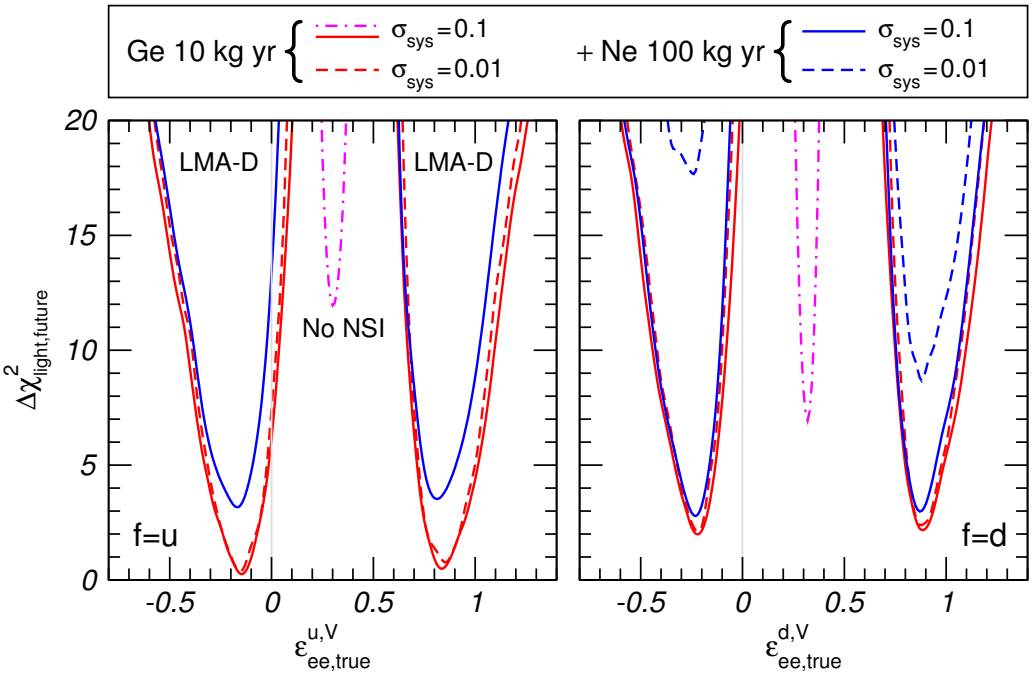

Figure 8. The full and dashed lines show $\Delta\chi^2_{\rm min}$(LMA-D) from a combination of current oscillation and future COHERENT data (for different assumptions on target and systematics as labeled) as a function of the assumed value of $\epsilon^{q,V}_{ee,\rm true}$. All other true values used to generate COHERENT data are set to the current best fit point from oscillations. To determine the minimum of the joint χ^2 in the LMA-D region all oscillation and NSI parameters are varied. The dash-dotted curve shows the $\Delta\chi^2$ for no-NSI under the same assumptions for our default COHERENT configuration.

high confidence. This is shown by the dot-dashed curve in figure 8, which gives the $\Delta\chi^2$ for the case with all $\epsilon^{q,V}_{\alpha\beta} = 0$. This curve does not reach zero because (a) oscillation data show some preference for non-zero NSI and give a contribution of $\Delta\chi^2 = 5.4$, see section 3.1, and (b) for any value of the assumed $\epsilon^{q,V}_{ee,\rm true}$ and assuming the oscillation best-fit to generate COHERENT data, the no-NSI point is disfavored at some level by COHERENT. But what is clear from the figure is that the no-NSI curve has no overlap with the regions where the LMA-D solution is a problem for COHERENT+oscillations. Hence, we conclude that if NSI exist with values such the LMA-D degeneracy remains, the combination of the present oscillation results with those from our default COHERENT set-up will tell us with high CL that non-zero NSI are present.

The same conclusion can be drawn from figure 7 for general values of $\epsilon^{q,V}_{ee}$ and $\epsilon^{q,V}_{\mu\mu}$, independent of the current best-fit point, by noting that the two dashed lines (along which the LMA-D degeneracy cannot be resolved) are "far" from the COHERENT solutions in case of no NSI and hence, parameter values along those lines can be distinguished from no NSI with high significance.

In principle the blind spots of COHERENT to the degeneracy shown in figure 8 could be lifted by using multiple nuclear targets since, as shown in appendix A, the locations of the blind spots depend on Z and N for the used nucleon. However, quantitatively the

JHEP04(2017)116

effect is rather small and adding Ar or Ne to Ge within our standard setup of COHERENT described in section 4 does not lead to much change. This is illustrated by the full blue line in figure 8. This line shows the $\Delta\chi^2_{\rm min}$ of the LMA-D region after adding data corresponding to 100 kg·yr exposure for ^{20}Ne (with a more conservative 10 keV threshold)[4] on top of the results obtained for our default ^{76}Ge configuration. We find that this combination can partially lift the degeneracy, but only when the systematic normalization error for each of these data samples is substantially reduced from our default 10% value. This is shown by the dashed blue curve in the figure where we show the results for the combination of ^{76}Ge and ^{20}Ne but reducing the systematic uncertainty down to a 1% systematic normalization uncertainty (which is taken to be completely uncorrelated between the two contributions to the COHERENT total χ^2).

Let us finally comment on the expected changes on these results if a coherent-scattering data from a reactor based experiment is used instead of the stopped pion source setup. In that case only the combination Q^2_{we} is determined, providing no constraint on $\epsilon^{q,V}_{\mu\mu}$. In this case, the degeneracy can be shifted completely in the $\mu\mu$ and $\tau\tau$ sector, and it will not be possible to lift the LMA-D degeneracy, for any true value of $\epsilon^{q,V}_{ee}$, see also appendix A. The situation is different in the heavy mediator case, where $\epsilon^{q,V}_{\mu\mu}$ is strongly constrained by NuTeV, as we will see below. In this case a coherent-scattering measurement at a reactor setup should suffice to rule out the LMA-D degeneracy.

5.2 NSI from a heavy mediator

Next we consider the case of NSI induced in models with a heavy mediator, as introduced in section 3.4. In this scenario, the scattering bounds from deep-inelastic neutrino-nucleus scattering would also apply. Thus, we construct a combined statistics including bounds from oscillations, CHARM, NuTeV, and the expected future contribution from COHERENT, as

$$\chi^2_{\rm heavy,future} = \chi^2_{\rm OSC} + \chi^2_{\rm CHARM} + \chi^2_{\rm NuTeV} + \chi^2_{\rm COH}\,. \tag{5.2}$$

Again in this case, to simulate the COHERENT data some assumption needs to be made regarding the input values of the NSI parameters. However, for this scenario the addition of NuTeV and CHARM to the oscillation data already provides very strong constraints on the NSI parameters (see figure 4) and, thus, the results obtained simulating COHERENT data for vanishing NSI, or for NSI according to the best-fit values of oscillation plus scattering, are very similar. Therefore, in this section we will only consider the case when COHERENT data are simulated using the SM as input (i.e., all NSI coefficients set to zero). A COHERENT configuration of 10 kg·yrs of ^{76}Ge, with a threshold of 5 keV for detection of nuclear recoils, will be considered as explained in more detail in section 4.

Figure 9 shows the dependence of $\Delta\chi^2_{\rm heavy,future}$ with all NSI coefficients (after marginalizing over all oscillation and NSI undisplayed parameters), for interactions with either up

[4]The choice of ^{20}Ne is not arbitrary. Among the considered targets for the COHERENT experiment, it gives the most different Z/N ratio compared to ^{76}Ge. This will provide the largest effect on the combined sensitivity.

JHEP04(2017)116

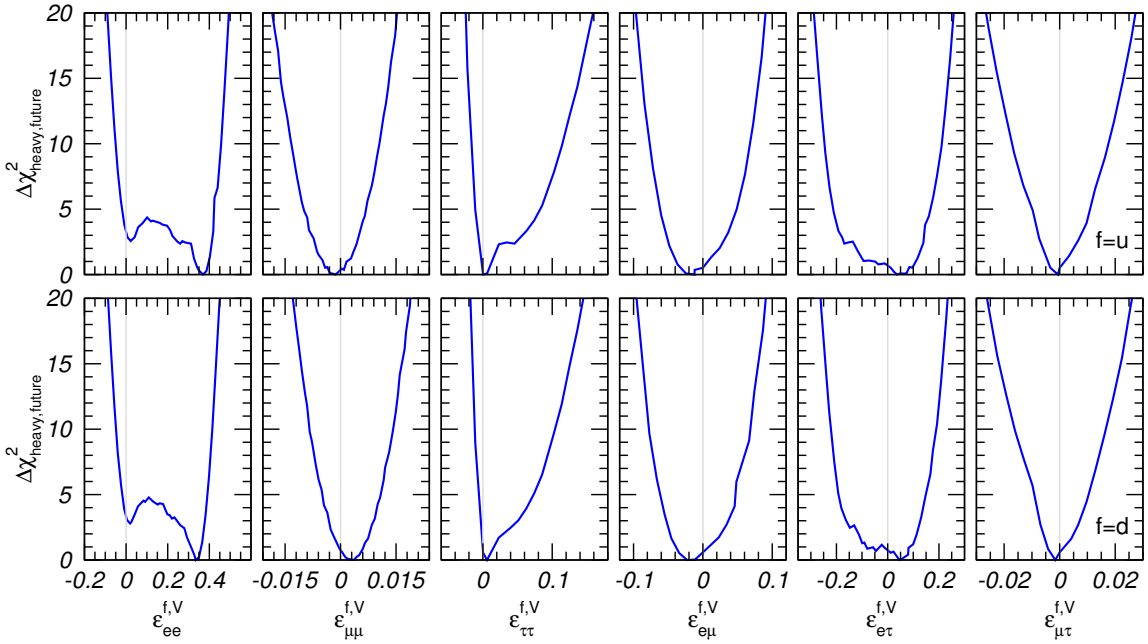

Figure 9. Dependence of $\Delta\chi^2_{\text{heavy,future}}$ on the NSI parameters $\epsilon^{f,V}_{\alpha\beta}$ for $f = u$ (upper panels) and $f = d$ (lower panels), using current global data on oscillations and DIS data from NuTeV and CHARM combined with artificial COHERENT data generated for all $\epsilon_{\alpha\beta}$ set to zero.

or down quarks as indicated by the labels. The corresponding allowed ranges at 90% CL are reported in table 1. As can be seen from the comparison between figure 9 and 4, the addition of COHERENT data allows to reject the LMA-D solution also in the $f = u$ scenario at high confidence level ($\Delta\chi^2_{\text{heavy,future,min}}(\text{LMA-D}) \sim 100$). For the LMA solution, the assumed configuration of COHERENT improves the determination of $\epsilon^{f,V}_{ee}$, while for all other NSI parameters we find no significant improvement compared to the present analysis of oscillations and scattering experiments.

6 Summary and conclusions

Non-Standard neutrino interactions (NSI) are generic expectations of physics beyond the standard model and can be parametrized in a model-independent approach in terms of dimension-six operators, which arise as the low-energy limit of some new interaction after integrating out its mediator. NSI modifying the charged-current leptonic interactions are currently strongly constrained by charged lepton data, while data on NSI affecting the neutral-current interactions (NSI-NC) of the neutrinos are sparse. At present current global fits to oscillation data provide some of the strongest constraints on NSI-NC, in particular for vector-like interactions which are those which affect the flavor evolution of the neutrinos in matter. Still, the results obtained in ref. [13] show that there remain two sets of solutions compatible with the data: the so-called LMA solution, as given in the SM extended with neutrino masses and mixing, compatible with negligible NSI, and a second one dubbed LMA-Dark [14] (or LMA-D), which requires large NSI and the solar

JHEP04(2017)116

Light			
PRESENT (OSC)		+COHERENT(SM)	
$\epsilon^{u,V}_{ee} - \epsilon^{u,V}_{\mu\mu}$	$[-1.19, -0.81] \oplus [0.00, 0.51]$	$\epsilon^{u,V}_{ee}$	$[0.002, 0.049] \oplus [0.28, 0.42]$
$\epsilon^{u,V}_{\tau\tau} - \epsilon^{u,V}_{\mu\mu}$	$[-0.03, 0.03]$	$\epsilon^{u,V}_{\mu\mu}$	$[-0.026, 0.033] \oplus [0.36, 0.38]$
		$\epsilon^{u,V}_{\tau\tau}$	$[-0.025, 0.047] \oplus [0.36, 0.39]$
$\epsilon^{u,V}_{e\mu}$	$[-0.09, 0.10]$	$[-0.08, 0.04]$	
$\epsilon^{u,V}_{e\tau}$	$[-0.15, 0.14]$	$[-0.17, 0.14]$	
$\epsilon^{u,V}_{\mu\tau}$	$[-0.01, 0.01]$	$[-0.01, 0.01]$	
$\epsilon^{d,V}_{ee} - \epsilon^{d,V}_{\mu\mu}$	$[-1.17, -1.03] \oplus [0.02, 0.51]$	$\epsilon^{d,V}_{ee}$	$[0.022, 0.023] \oplus [0.25, 0.38]$
$\epsilon^{d,V}_{\tau\tau} - \epsilon^{d,V}_{\mu\mu}$	$[-0.01, 0.03]$	$\epsilon^{d,V}_{\mu\mu}$	$[-0.024, 0.029]$
		$\epsilon^{d,V}_{\tau\tau}$	$[-0.023, 0.039]$
$\epsilon^{d,V}_{e\mu}$	$[-0.09, 0.08]$	$[-0.07, 0.04]$	
$\epsilon^{d,V}_{e\tau}$	$[-0.13, 0.14]$	$[-0.14, 0.12]$	
$\epsilon^{d,V}_{\mu\tau}$	$[-0.01, 0.01]$	$[-0.009, 0.007]$	
Heavy			
PRESENT (OSC+CHARM+NuTeV)		+COHERENT(SM)	
$\epsilon^{u,V}_{ee}$	$[-0.97, -0.83] \oplus [0.033, 0.450]$	$[0.014, 0.032] \oplus [0.24, 0.41]$	
$\epsilon^{u,V}_{\mu\mu}$	$[-0.008, 0.005]$	$[-0.007, 0.005]$	
$\epsilon^{u,V}_{\tau\tau}$	$[-0.015, 0.04]$	$[-0.006, 0.04]$	
$\epsilon^{u,V}_{e\mu}$	$[-0.05, 0.03]$	$[-0.05, 0.03]$	
$\epsilon^{u,V}_{e\tau}$	$[-0.15, 0.13]$	$[-0.15, 0.13]$	
$\epsilon^{u,V}_{\mu\tau}$	$[-0.006, 0.005]$	$[-0.006, 0.004]$	
$\epsilon^{d,V}_{ee}$	$[0.02, 0.51]$	$[0.26, 0.38]$	
$\epsilon^{d,V}_{\mu\mu}$	$[-0.003, 0.009]$	$[-0.003, 0.009]$	
$\epsilon^{d,V}_{\tau\tau}$	$[-0.001, 0.05]$	$[-0.001, 0.05]$	
$\epsilon^{d,V}_{e\mu}$	$[-0.05, 0.03]$	$[-0.05, 0.03]$	
$\epsilon^{d,V}_{e\tau}$	$[-0.15, 0.14]$	$[-0.15, 0.14]$	
$\epsilon^{d,V}_{\mu\tau}$	$[-0.007, 0.007]$	$[-0.007, 0.007]$	

Table 1. 90% and allowed ranges for the NSI parameters $\epsilon^f_{\alpha\beta}$ for $f = u, d$ as obtained from the different combined analyses. The upper (lower) part of the table corresponds to models of NSI's generated by light (heavy) mediators. The results in each panel are obtained after marginalizing over oscillation and the other NSI parameters. See text for details.

mixing angle to lie in the upper octant. Currently, the two solutions (LMA and LMA-D) are almost completely degenerate, the fit showing only a slight preference for the LMA solution with $\Delta\chi^2 \sim 0.2(2)$ for the NSI with up (down) quarks.

The LMA-D solution is a consequence of a more profound degeneracy which affects the Hamiltonian governing neutrino oscillations. This degeneracy involves a change in the

JHEP04(2017)116

matter potential and a change in the octant of the solar angle, but it also needs a change in the CP-phase δ and a flip in the neutrino mass ordering. Besides, it takes place regardless of whether the experiment is performed in vacuum or in presence of a matter potential. Therefore, this degeneracy will make it impossible to determine the neutrino mass ordering at neutrino oscillation experiments unless it is ruled out by other experiments first.

Other processes capable of constraining NSI-NC include neutrino-nucleus deep-inelastic scattering. At present, the most precise results come from NuTeV and CHARM and provide constraints for NSI affecting ν_μ and ν_e respectively. Since oscillation data is only sensitive to differences among diagonal couplings, the combination with scattering data is crucial to obtain independent bounds for all parameters entering the matter potential separately. In this work, we have performed a global fit to oscillation and scattering data from the NuTeV and CHARM experiments, deriving the strongest constraints on neutral-current NSI in the literature. The fit was done including all vector NSI operators affecting either up or down quarks at a time. Marginalization over the standard oscillation parameters has been performed. Our results for this fit are summarized in figure 4, while the limits at the 90% CL are listed in table 1. The combination with scattering data also rules out the LMA-D solution for NSI involving down quarks, as pointed out earlier [14, 20]. However, we show that the LMA-D solution still survives for NSI with up quarks.

Nevertheless, as we have stressed, the NuTeV and CHARM bounds are not applicable to all models leading to NSI in the neutrino sector. For example, if the NSI come from neutrino interactions with a new light mediator, the bounds derived from deep-inelastic processes will be strongly suppressed with the inverse of the momentum transfer and can be evaded. In this case, only oscillation data would be applicable. Future neutrino-nucleus coherent scattering experiments will also be able to put additional constraints. As coherent neutrino-nucleus scattering involves a much lower momentum transfer, such bounds would be applicable in models with light mediators. Thus, in the second part of our work, we have explored the impact of the results expected from such experiments on the limits to NSI operators taking as an example the COHERENT experiment with a ^{76}Ge detector with 5 keV threshold and 10 kg·yrs exposure at a stopped pion source. We have distinguished explicitly two cases: NSI models with heavy mediators (where bounds from oscillation data, NuTeV and CHARM would apply) and models with light mediators (where only present oscillation bounds would apply). In order to generate COHERENT data, we have used two assumptions: (i) the data are obtained under the assumption of no NSI, and (ii) the data are obtained using the best-fit NSI values from a global fit to previous experiments. Our results are summarized in figures 9 for the heavy mediator case, and in figures 6 and 8 for the light mediator case. The expected 90% CL ranges are summarized in table 1.

In the case of NSI from light mediators, we find that the combination of COHERENT and current experiments should be able to definitely rule out the LMA-D solution also in the case of NSI with up quarks, as long as the results of COHERENT are as expected for negligible NSI (case i above). However, if COHERENT data is instead in agreement with the expectations from the current best-fit point of oscillations it may not be possible to rule out the LMA-D solution, as clearly illustrated in figure 8. This is a consequence of the presence of degeneracies in the NSI parameters allowed by COHERENT, as we detail in

JHEP04(2017)116

appendix A. We find that breaking those and fully ruling out the LMA-D may be achieved by a combination of coherent scattering data with different nuclei, but only if very good control of the systematics affecting the normalization of the event rates can be achieved. However, one must realize that, even in scenarios for which the LMA-D degeneracy cannot be lifted, the experiment will be able to rule out the no-NSI hypothesis at high CL and discover the presence of new interactions in the neutrino sector.

Conversely, in the heavy mediator case, when CHARM and NuTeV constraints apply, adding COHERENT data will rule out the LMA-D region also for the case of NSI with up quarks. Hence, in this case it is always possible to completely resolve the degeneracy.

Acknowledgments

We warmly thank Kate Scholberg for useful discussions and for providing us with the form factors needed to simulate the COHERENT experiment. This work is supported by USA-NSF grant PHY-1620628, by EU Networks FP10 ITN ELUSIVES (H2020-MSCA-ITN-2015-674896) and INVISIBLES-PLUS (H2020-MSCA-RISE-2015-690575), by MINECO grant FPA2013-46570 and MINECO/FEDER-UE grants FPA2015-65929-P and FPA2016-78645-P, by Maria de Maetzu program grant MDM-2014-0367 of ICCUB, by the "Severo Ochoa" program grant SEV-2012-0249 of IFT, by the Fermilab Graduate Student Research Program in Theoretical Physics operated by Fermi Research Alliance, LLC, by the Villum Foundation (Project No. 13164), and by the Danish National Research Foundation (DNRF91). Fermilab is operated by Fermi Research Alliance, LLC under Contract No. DE-AC02-07CH11359 with the United States Department of Energy.

A Resolving LMA-D by COHERENT data

In this appendix we provide an analytic discussion of the ability to resolve the LMA-D degeneracy using a combination of oscillation and coherent-scattering data, i.e., we focus on light NSI mediators.

In a coherent scattering experiment at a stopped pion source, two combinations of e- and μ-like events can be measured by using timing information, see section 4. Hence, an ideal experiment would be able to extract both the electron- and muon-neutrino scattering cross sections. Effectively the two parameter combinations Q^2_{we} and $Q^2_{w\mu}$ given in eq. (4.3) can be measured. Let us set all off-diagonal NSI to zero and assume that NSI happen either with up or down quarks. Then we can write

$$Q^2_{w\alpha} \propto (X_q - \epsilon^{q,V}_{\alpha\alpha})^2 \,, \tag{A.1}$$

with

$$X_u = -\frac{Z g^{p,V} + N g^{n,V}}{2Z + N} \,, \qquad X_d = -\frac{Z g^{p,V} + N g^{n,V}}{Z + 2N} \,. \tag{A.2}$$

We now introduce the following notation:

$$\begin{aligned} s_q &= \epsilon^{q,V}_{ee} + \epsilon^{q,V}_{\mu\mu} \,, \\ d_q &= \epsilon^{q,V}_{ee} - \epsilon^{q,V}_{\mu\mu} \,. \end{aligned} \tag{A.3}$$

JHEP04(2017)116

Oscillations are sensitive only to d_q, with best-fit $d_q \approx 0.3$, and the LMA-D degenerate solution at $d'_q = -d_q - \xi_q$ according to eq. (2.5), with the ξ_q given in eq. (3.1). COHERENT depends also on s_q. The transformation $d_q \to d'_q$ can be supplemented by $s_q \to s'_q$. If we can arrange s_q and s'_q such that

$$\begin{aligned} [2X_q - (s_q + d_q)]^2 &= \left[2X_q - (s'_q + d'_q)\right]^2 , \\ [2X_q - (s_q - d_q)]^2 &= \left[2X_q - (s'_q - d'_q)\right]^2 , \end{aligned} \tag{A.4}$$

then COHERENT will be affected by the degeneracy as well. We use $d'_q = -d_q - \xi_q$ and take the square root of the above equations. The two non-trivial sign combinations lead to

$$\begin{aligned} 2X_q - (s_q + d_q) &= \pm \left[2X_q - (s'_q - d_q - \xi_q)\right] , \\ 2X_q - (s_q - d_q) &= \mp \left[2X_q - (s'_q + d_q + \xi_q)\right] . \end{aligned} \tag{A.5}$$

Using only information from oscillations, the sum s_q is unknown. So we can consider those equations for the two unknowns s_q and s'_q. In particular we find

$$s_q = 2X_q \mp (d_q + \xi_q) , \tag{A.6}$$

which implies

$$\epsilon_{ee}^{q,V} = \begin{cases} X_q - \xi_q/2 \\ X_q + \xi_q/2 + d_q \end{cases} \quad \text{or} \quad \begin{aligned} \epsilon_{ee}^{q,V} &= X_q - \xi_q/2 \\ \epsilon_{\mu\mu}^{q,V} &= X_q + \xi_q/2 \end{aligned} . \tag{A.7}$$

Numerically we obtain

$$\epsilon_{ee}^{u,V} = \begin{cases} -0.150 \\ 0.842 \end{cases} \qquad \epsilon_{ee}^{d,V} = \begin{cases} -0.224 \\ 0.886 \end{cases} , \tag{A.8}$$

where we used $d_u = 0.307, d_d = 0.316$ from the best-fit values for oscillation data, and we took $Z = 32, N = 44$ for ^{76}Ge. The values for $\epsilon_{ee}^{u,V}$ and $\epsilon_{\mu\mu}^{u,V}$ following from eq. (A.7) are shown as the dashed lines in figure 7. If those are the true values for $\epsilon_{ee}^{q,V}$ or $\epsilon_{\mu\mu}^{q,V}$, COHERENT will not be able to resolve the degeneracy. Those estimates are in excellent agreement with the numerical results shown in figure 8. We can make the following comments:

- If there are no NSI in Nature ($d_q = s_q = 0$), eqs. (A.5) cannot be fulfilled, which implies that the degeneracy is resolved, in agreement with figure 6. This follows also from the fact that the dashed lines in figure 7 do not pass close to the SM point.

- If we use a reactor instead of the stopped pion source for the coherent scattering experiment, only the first equation in (A.5) applies (corresponding to Q^2_{we}). For given d_q and s_q there is always a solution for s'_q. Hence, a reactor experiment combined with oscillation data cannot resolve the degeneracy in the light mediator case.

- For a different target nucleus, the values of X_q change. Hence, eqs. (A.5) cannot be fulfilled simultaneously for two targets and in principle the degeneracy can be resolved by using different target nuclei. However, as discussed in the context of figure 8, the effect is small and exploring it to resolve the degeneracy may be experimentally challenging.

JHEP04(2017)116

References

[1] B. Pontecorvo, *Neutrino Experiments and the Problem of Conservation of Leptonic Charge*, *Sov. Phys. JETP* **26** (1968) 984 [INSPIRE].

[2] V.N. Gribov and B. Pontecorvo, *Neutrino astronomy and lepton charge*, *Phys. Lett.* **28B** (1969) 493 [INSPIRE].

[3] Z. Maki, M. Nakagawa and S. Sakata, *Remarks on the unified model of elementary particles*, *Prog. Theor. Phys.* **28** (1962) 870 [INSPIRE].

[4] I. Esteban, M.C. Gonzalez-Garcia, M. Maltoni, I. Martinez-Soler and T. Schwetz, *Updated fit to three neutrino mixing: exploring the accelerator-reactor complementarity*, *JHEP* **01** (2017) 087 [arXiv:1611.01514] [INSPIRE].

[5] S. Weinberg, *Baryon and Lepton Nonconserving Processes*, *Phys. Rev. Lett.* **43** (1979) 1566 [INSPIRE].

[6] L. Wolfenstein, *Neutrino Oscillations in Matter*, *Phys. Rev.* **D 17** (1978) 2369 [INSPIRE].

[7] J.W.F. Valle, *Resonant Oscillations of Massless Neutrinos in Matter*, *Phys. Lett.* **B 199** (1987) 432 [INSPIRE].

[8] M.M. Guzzo, A. Masiero and S.T. Petcov, *On the MSW effect with massless neutrinos and no mixing in the vacuum*, *Phys. Lett.* **B 260** (1991) 154 [INSPIRE].

[9] T. Ohlsson, *Status of non-standard neutrino interactions*, *Rept. Prog. Phys.* **76** (2013) 044201 [arXiv:1209.2710] [INSPIRE].

[10] O.G. Miranda and H. Nunokawa, *Non standard neutrino interactions: current status and future prospects*, *New J. Phys.* **17** (2015) 095002 [arXiv:1505.06254] [INSPIRE].

[11] S.P. Mikheev and A.Yu. Smirnov, *Resonance Amplification of Oscillations in Matter and Spectroscopy of Solar Neutrinos*, *Sov. J. Nucl. Phys.* **42** (1985) 913 [INSPIRE].

[12] M.C. Gonzalez-Garcia, M. Maltoni and J. Salvado, *Testing matter effects in propagation of atmospheric and long-baseline neutrinos*, *JHEP* **05** (2011) 075 [arXiv:1103.4365] [INSPIRE].

[13] M.C. Gonzalez-Garcia and M. Maltoni, *Determination of matter potential from global analysis of neutrino oscillation data*, *JHEP* **09** (2013) 152 [arXiv:1307.3092] [INSPIRE].

[14] O.G. Miranda, M.A. Tortola and J.W.F. Valle, *Are solar neutrino oscillations robust?*, *JHEP* **10** (2006) 008 [hep-ph/0406280] [INSPIRE].

[15] P. Bakhti and Y. Farzan, *Shedding light on LMA-Dark solar neutrino solution by medium baseline reactor experiments: JUNO and RENO-50*, *JHEP* **07** (2014) 064 [arXiv:1403.0744] [INSPIRE].

[16] P. Coloma and T. Schwetz, *Generalized mass ordering degeneracy in neutrino oscillation experiments*, *Phys. Rev.* **D 94** (2016) 055005 [arXiv:1604.05772] [INSPIRE].

[17] S. Davidson, C. Pena-Garay, N. Rius and A. Santamaria, *Present and future bounds on nonstandard neutrino interactions*, *JHEP* **03** (2003) 011 [hep-ph/0302093] [INSPIRE].

[18] C. Biggio, M. Blennow and E. Fernandez-Martinez, *General bounds on non-standard neutrino interactions*, *JHEP* **08** (2009) 090 [arXiv:0907.0097] [INSPIRE].

JHEP04(2017)116

[19] C. Biggio, M. Blennow and E. Fernandez-Martinez, *Loop bounds on non-standard neutrino interactions*, *JHEP* **03** (2009) 139 [arXiv:0902.0607] [INSPIRE].

[20] F.J. Escrihuela, O.G. Miranda, M.A. Tortola and J.W.F. Valle, *Constraining nonstandard neutrino-quark interactions with solar, reactor and accelerator data*, *Phys. Rev.* **D 80** (2009) 105009 [*Erratum ibid.* **D 80** (2009) 129908] [arXiv:0907.2630] [INSPIRE].

[21] COHERENT collaboration, D. Akimov et al., *The COHERENT Experiment at the Spallation Neutron Source*, arXiv:1509.08702 [INSPIRE].

[22] H.T. Wong, *Ultra-Low-Energy Germanium Detector for Neutrino-Nucleus Coherent Scattering and Dark Matter Searches*, *Mod. Phys. Lett.* **A 23** (2008) 1431 [arXiv:0803.0033] [INSPIRE].

[23] CONNIE collaboration, A. Aguilar-Arevalo et al., *The CONNIE experiment*, *J. Phys. Conf. Ser.* **761** (2016) 012057 [arXiv:1608.01565] [INSPIRE].

[24] CONNIE collaboration, A. Aguilar-Arevalo et al., *Results of the engineering run of the Coherent Neutrino Nucleus Interaction Experiment (CONNIE)*, 2016 *JINST* **11** P07024 [arXiv:1604.01343] [INSPIRE].

[25] MINER collaboration, G. Agnolet et al., *Background Studies for the MINER Coherent Neutrino Scattering Reactor Experiment*, *Nucl. Instrum. Meth.* **A 853** (2017) 53 [arXiv:1609.02066] [INSPIRE].

[26] J. Billard et al., *Coherent Neutrino Scattering with Low Temperature Bolometers at CHOOZ Reactor Complex*, arXiv:1612.09035 [INSPIRE].

[27] D.G. Cerdeño, M. Fairbairn, T. Jubb, P.A.N. Machado, A.C. Vincent and C. Bœhm, *Physics from solar neutrinos in dark matter direct detection experiments*, *JHEP* **05** (2016) 118 [*Erratum ibid.* **09** (2016) 048] [arXiv:1604.01025] [INSPIRE].

[28] CHARM collaboration, J. Dorenbosch et al., *Experimental Verification of the Universality of ν_e and ν_μ Coupling to the Neutral Weak Current*, *Phys. Lett.* **B 180** (1986) 303 [INSPIRE].

[29] NuTeV collaboration, G.P. Zeller et al., *A Precise determination of electroweak parameters in neutrino nucleon scattering*, *Phys. Rev. Lett.* **88** (2002) 091802 [*Erratum ibid.* **90** (2003) 239902] [hep-ex/0110059] [INSPIRE].

[30] M. Kobayashi and T. Maskawa, *CP Violation in the Renormalizable Theory of Weak Interaction*, *Prog. Theor. Phys.* **49** (1973) 652 [INSPIRE].

[31] M.B. Gavela, D. Hernandez, T. Ota and W. Winter, *Large gauge invariant non-standard neutrino interactions*, *Phys. Rev.* **D 79** (2009) 013007 [arXiv:0809.3451] [INSPIRE].

[32] S. Antusch, J.P. Baumann and E. Fernandez-Martinez, *Non-Standard Neutrino Interactions with Matter from Physics Beyond the Standard Model*, *Nucl. Phys.* **B 810** (2009) 369 [arXiv:0807.1003] [INSPIRE].

[33] M.B. Wise and Y. Zhang, *Effective Theory and Simple Completions for Neutrino Interactions*, *Phys. Rev.* **D 90** (2014) 053005 [arXiv:1404.4663] [INSPIRE].

[34] C. Bœhm, *Implications of a new light gauge boson for neutrino physics*, *Phys. Rev.* **D 70** (2004) 055007 [hep-ph/0405240] [INSPIRE].

[35] Y. Farzan, *A model for large non-standard interactions of neutrinos leading to the LMA-Dark solution*, *Phys. Lett.* **B 748** (2015) 311 [arXiv:1505.06906] [INSPIRE].

[36] Y. Farzan and I.M. Shoemaker, *Lepton Flavor Violating Non-Standard Interactions via Light Mediators*, *JHEP* **07** (2016) 033 [arXiv:1512.09147] [INSPIRE].

JHEP04(2017)116

[37] Y. Farzan and J. Heeck, *Neutrinophilic nonstandard interactions*, *Phys. Rev.* **D 94** (2016) 053010 [arXiv:1607.07616] [INSPIRE].

[38] D.V. Forero and W.-C. Huang, *Sizable NSI from the* $SU(2)_L$ *scalar doublet-singlet mixing and the implications in DUNE*, *JHEP* **03** (2017) 018 [arXiv:1608.04719] [INSPIRE].

[39] A. Friedland, M.L. Graesser, I.M. Shoemaker and L. Vecchi, *Probing Nonstandard Standard Model Backgrounds with LHC Monojets*, *Phys. Lett.* **B 714** (2012) 267 [arXiv:1111.5331] [INSPIRE].

[40] D. Buarque Franzosi, M.T. Frandsen and I.M. Shoemaker, *New or* ν *missing energy: Discriminating dark matter from neutrino interactions at the LHC*, *Phys. Rev.* **D 93** (2016) 095001 [arXiv:1507.07574] [INSPIRE].

[41] KamLAND collaboration, A. Gando et al., *Constraints on* θ_{13} *from A Three-Flavor Oscillation Analysis of Reactor Antineutrinos at KamLAND*, *Phys. Rev.* **D 83** (2011) 052002 [arXiv:1009.4771] [INSPIRE].

[42] B.T. Cleveland et al., *Measurement of the solar electron neutrino flux with the Homestake chlorine detector*, *Astrophys. J.* **496** (1998) 505 [INSPIRE].

[43] F. Kaether, W. Hampel, G. Heusser, J. Kiko and T. Kirsten, *Reanalysis of the GALLEX solar neutrino flux and source experiments*, *Phys. Lett.* **B 685** (2010) 47 [arXiv:1001.2731] [INSPIRE].

[44] SAGE collaboration, J.N. Abdurashitov et al., *Measurement of the solar neutrino capture rate with gallium metal. III: Results for the 2002–2007 data-taking period*, *Phys. Rev.* **C 80** (2009) 015807 [arXiv:0901.2200] [INSPIRE].

[45] Super-Kamiokande collaboration, J. Hosaka et al., *Solar neutrino measurements in Super-Kamiokande-I*, *Phys. Rev.* **D 73** (2006) 112001 [hep-ex/0508053] [INSPIRE].

[46] Super-Kamiokande collaboration, J.P. Cravens et al., *Solar neutrino measurements in Super-Kamiokande-II*, *Phys. Rev.* **D 78** (2008) 032002 [arXiv:0803.4312] [INSPIRE].

[47] Super-Kamiokande collaboration, K. Abe et al., *Solar neutrino results in Super-Kamiokande-III*, *Phys. Rev.* **D 83** (2011) 052010 [arXiv:1010.0118] [INSPIRE].

[48] Super-Kamiokande collaboration, M. Smy, *Super-Kamiokande's solar* ν *results*, *Nucl. Phys. Proc. Suppl.* **235-236** (2013) 49 [INSPIRE].

[49] G. Bellini et al., *Precision measurement of the 7Be solar neutrino interaction rate in Borexino*, *Phys. Rev. Lett.* **107** (2011) 141302 [arXiv:1104.1816] [INSPIRE].

[50] Borexino collaboration, G. Bellini et al., *Measurement of the solar 8B neutrino rate with a liquid scintillator target and 3 MeV energy threshold in the Borexino detector*, *Phys. Rev.* **D 82** (2010) 033006 [arXiv:0808.2868] [INSPIRE].

[51] SNO collaboration, B. Aharmim et al., *Determination of the* ν_e *and total* ^8B *solar neutrino fluxes with the Sudbury neutrino observatory phase I data set*, *Phys. Rev.* **C 75** (2007) 045502 [nucl-ex/0610020] [INSPIRE].

[52] SNO collaboration, B. Aharmim et al., *Electron energy spectra, fluxes and day-night asymmetries of B-8 solar neutrinos from measurements with NaCl dissolved in the heavy-water detector at the Sudbury Neutrino Observatory*, *Phys. Rev.* **C 72** (2005) 055502 [nucl-ex/0502021] [INSPIRE].

[53] SNO collaboration, B. Aharmim et al., *An Independent Measurement of the Total Active B-8 Solar Neutrino Flux Using an Array of He-3 Proportional Counters at the Sudbury Neutrino Observatory*, *Phys. Rev. Lett.* **101** (2008) 111301 [arXiv:0806.0989] [INSPIRE].

JHEP04(2017)116

[54] SNO collaboration, B. Aharmim et al., *Combined Analysis of all Three Phases of Solar Neutrino Data from the Sudbury Neutrino Observatory*, *Phys. Rev.* **C 88** (2013) 025501 [arXiv:1109.0763] [INSPIRE].

[55] L.K. Pik, *Study of the neutrino mass hierarchy with the atmospheric neutrino data observed in Super-Kamiokande*, Ph.D. Thesis, University of Tokyo (2012) [INSPIRE].

[56] MINOS collaboration, P. Adamson et al., *Measurement of Neutrino and Antineutrino Oscillations Using Beam and Atmospheric Data in MINOS*, *Phys. Rev. Lett.* **110** (2013) 251801 [arXiv:1304.6335] [INSPIRE].

[57] MINOS collaboration, P. Adamson et al., *Electron neutrino and antineutrino appearance in the full MINOS data sample*, *Phys. Rev. Lett.* **110** (2013) 171801 [arXiv:1301.4581] [INSPIRE].

[58] M. Ikeda, *Recent results from T2K*, in *Rencontres de Moriond EW*, 2–9 March 2013.

[59] CHOOZ collaboration, M. Apollonio et al., *Limits on neutrino oscillations from the CHOOZ experiment*, *Phys. Lett.* **B 466** (1999) 415 [hep-ex/9907037] [INSPIRE].

[60] Palo Verde collaboration, A. Piepke, *Final results from the Palo Verde neutrino oscillation experiment*, *Prog. Part. Nucl. Phys.* **48** (2002) 113 [INSPIRE].

[61] Double CHOOZ collaboration, Y. Abe et al., *Reactor electron antineutrino disappearance in the Double CHOOZ experiment*, *Phys. Rev.* **D 86** (2012) 052008 [arXiv:1207.6632] [INSPIRE].

[62] Daya Bay collaboration, F.P. An et al., *Improved Measurement of Electron Antineutrino Disappearance at Daya Bay*, *Chin. Phys.* **C 37** (2013) 011001 [arXiv:1210.6327] [INSPIRE].

[63] S.H. Seo, *RENO*, PoS(Neutel 2013)018.

[64] Y. Declais et al., *Study of reactor anti-neutrino interaction with proton at Bugey nuclear power plant*, *Phys. Lett.* **B 338** (1994) 383 [INSPIRE].

[65] Y. Declais et al., *Search for neutrino oscillations at 15-meters, 40-meters and 95-meters from a nuclear power reactor at Bugey*, *Nucl. Phys.* **B 434** (1995) 503 [INSPIRE].

[66] A.A. Kuvshinnikov, L.A. Mikaelyan, S.V. Nikolaev, M.D. Skorokhvatov and A.V. Etenko, *Measuring the anti-electron-neutrino* $+p \to n + e^+$ *cross-section and beta decay axial constant in a new experiment at Rovno NPP reactor* (in Russian), *JETP Lett.* **54** (1991) 253 [INSPIRE].

[67] A.I. Afonin, S.N. Ketov, V.I. Kopeikin, L.A. Mikaelyan, M.D. Skorokhvatov and S.V. Tolokonnikov, *A Study of the Reaction* $\bar{\nu}_e + P \to e^+ + N$ *on a Nuclear Reactor*, *Sov. Phys. JETP* **67** (1988) 213 [INSPIRE].

[68] G.S. Vidyakin et al., *Detection of Anti-neutrinos in the Flux From Two Reactors*, *Sov. Phys. JETP* **66** (1987) 243 [INSPIRE].

[69] G.S. Vidyakin et al., *Limitations on the characteristics of neutrino oscillations*, *JETP Lett.* **59** (1994) 390 [INSPIRE].

[70] H. Kwon et al., *Search for Neutrino Oscillations at a Fission Reactor*, *Phys. Rev.* **D 24** (1981) 1097 [INSPIRE].

[71] CALTECH-SIN-TUM collaboration, G. Zacek et al., *Neutrino Oscillation Experiments at the Gosgen Nuclear Power Reactor*, *Phys. Rev.* **D 34** (1986) 2621 [INSPIRE].

[72] Z.D. Greenwood et al., *Results of a two position reactor neutrino oscillation experiment*, *Phys. Rev.* **D 53** (1996) 6054 [INSPIRE].

JHEP04(2017)116

[73] A. Friedland, C. Lunardini and M. Maltoni, *Atmospheric neutrinos as probes of neutrino-matter interactions*, *Phys. Rev.* **D 70** (2004) 111301 [hep-ph/0408264] [INSPIRE].

[74] J. Erler and S. Su, *The Weak Neutral Current*, *Prog. Part. Nucl. Phys.* **71** (2013) 119 [arXiv:1303.5522] [INSPIRE].

[75] G.P. Zeller, *A precise measurement of the weak mixing angle in neutrino-nucleon scattering*, Ph.D. Thesis, Northwestern U. (2002) [INSPIRE].

[76] NNPDF collaboration, R.D. Ball et al., *Precision determination of electroweak parameters and the strange content of the proton from neutrino deep-inelastic scattering*, *Nucl. Phys.* **B 823** (2009) 195 [arXiv:0906.1958] [INSPIRE].

[77] W. Bentz, I.C. Cloet, J.T. Londergan and A.W. Thomas, *Reassessment of the NuTeV determination of the weak mixing angle*, *Phys. Lett.* **B 693** (2010) 462 [arXiv:0908.3198] [INSPIRE].

[78] J. Barranco, O.G. Miranda and T.I. Rashba, *Probing new physics with coherent neutrino scattering off nuclei*, *JHEP* **12** (2005) 021 [hep-ph/0508299] [INSPIRE].

[79] K. Scholberg, *Prospects for measuring coherent neutrino-nucleus elastic scattering at a stopped-pion neutrino source*, *Phys. Rev.* **D 73** (2006) 033005 [hep-ex/0511042] [INSPIRE].

[80] M. Lindner, W. Rodejohann and X.-J. Xu, *Coherent Neutrino-Nucleus Scattering and new Neutrino Interactions*, *JHEP* **03** (2017) 097 [arXiv:1612.04150] [INSPIRE].

[81] J.B. Dent, B. Dutta, S. Liao, J.L. Newstead, L.E. Strigari and J.W. Walker, *Probing light mediators at ultra-low threshold energies with coherent elastic neutrino-nucleus scattering*, arXiv:1612.06350 [INSPIRE].

[82] R.L. Kustom, *An Overview of the Spallation Neutron Source project*, *eConf* **C 000821** (2000) TU101 [physics/0008212] [INSPIRE].

[83] R. Cooper, *COHERENT at the Spallation Neutron Source*, in *International Conference of High Energy Physics*, (2016).

[84] C.J. Horowitz, K.J. Coakley and D.N. McKinsey, *Supernova observation via neutrino-nucleus elastic scattering in the CLEAN detector*, *Phys. Rev.* **D 68** (2003) 023005 [astro-ph/0302071] [INSPIRE].

JHEP04(2017)116